Fractional cyber-neural systems – a brief survey*

Emily Reed*a, Sarthak Chatterjee*b, Guilherme Ramos*c, Paul Bogdana, Sérgio Pequitod

^aMing Hsieh Department of Electrical and Computer Engineering, University of Southern California, Los Angeles, CA, USA

Abstract

Neurotechnology has made great strides in the last 20 years. However, we still have a long way to go to commercialize many of these technologies as we lack a unified framework to study cyber-neural systems (CNS) that bring the hardware, software, and the neural system together. Dynamical systems play a key role in developing these technologies as they capture different aspects of the brain and provide insight into their function. Converging evidence suggests that fractional-order dynamical systems are advantageous in modeling neural systems because of their compact representation and accuracy in capturing the long-range memory exhibited in neural behavior. In this brief

^bDepartment of Electrical, Computer, and Systems Engineering, Rensselaer Polytechnic Institute, Troy, NY, USA

^cDepartment of Electrical and Computer Engineering, Faculty of Engineering, University of Porto, Portugal

^dDelft Center for Systems and Control, Delft University of Technology, Delft, The Netherlands

^{*}This work was supported in part by FCT project POCI-01-0145-FEDER-031411-HARMONY, National Science Foundation GRFP DGE-1842487, Career Award CPS/CNS-1453860, CCF-1837131, MCB-1936775, CNS-1932620, CMMI-1936624, CMMI-1936578, the University of Southern California Annenberg Fellowship, USC WiSE Top-Off Fellowship, the DARPA Young Faculty Award and DARPA Director Award N66001-17-1-4044. The views, opinions, and/or findings contained in this article are those of the authors and should not be interpreted as representing the official views or policies, either expressed or implied by the Defense Advanced Research Projects Agency, the Department of Defense, or the National Science Foundation.

^{*}The first three authors contributed equally.

Email addresses: emilyree@usc.edu (Emily Reed*), sarthak.chatterjee92@gmail.com (Sarthak Chatterjee*), guilhermeramos21@gmail.com (Guilherme Ramos*), pbogdan@usc.edu (Paul Bogdan), Sergio.Pequito@tudelft.nl (Sérgio Pequito)

survey, we provide an overview of fractional CNS that entails fractional-order systems in the context of CNS. In particular, we introduce basic definitions required for the analysis and synthesis of fractional CNS, encompassing system identification, state estimation, and closed-loop control. Additionally, we provide an illustration of some applications in the context of CNS and draw some possible future research directions. Ultimately, advancements in these three areas will be critical in developing the next generation of CNS, which will, ultimately, improve people's quality of life.

Keywords: fractional-order systems, cyber-neural systems, neurotechnology

Contents

1	Introduction 1.1 Continuous-time fractional order systems 1.2 Discrete-time fractional-order systems 1.3 Paper organization	3 6 8 10
2	Stability	10
3	Controllability and observability	11
4	Proportional-integral-derivative control	14
5	Sliding mode control	15
6	Backstepping control	19
7	Adaptive control	21
8	System identification	22
9	Minimum-energy state estimation	27
10	Fractional optimal control	33
11	Model predictive control	34
12	Applications in cyber-neural systems 12.1 System identification	36 36 37 39 40 42
13	Conclusions and directions for future research 13.1 System identification	47 47 48 49

1. Introduction

We have witnessed an increase in the popularity of neurotechnology, in part propelled by several Silicon Valley companies such as NeuraLink (Regalado, 2020) (founded by Elon Musk), Google, and Facebook, just to mention a few. This tendency is now emerging in Europe as well with a variety of start-up companies across different countries. Yet, we have a long path moving forward to commercialize these devices to a clinical domain (Lewis, 2020; Carmena et al., 2019; Chavarriaga, 2020). Among the different neurotechnologies, the one experiencing the biggest growth is that of neurostimulation devices to assess the neural activity (e.g., by tracking the change in electrical potential) and to inject a timely stimulus (e.g., current in electrical neurostimulation devices) that aims to disrupt such activity (Rodgers, 2020). These devices consist of tightly integrated hardware/software components and together with the neural system that they monitor and regulate they form a cyber-neural system (CNS).

Neural systems like the brain generally exhibit quite diverse activity patterns across subjects under different operational setups (Bargmann et al., 2014). Therefore, it is important to develop and translate the tools to enable CNS to become tomorrow's reality. Yet, to several scientists and engineers, this is the 21st century equivalent of the space race that led the man to the moon. Consequently, it is imperative to establish a unified robust framework to understand and regulate brain activity across individuals and regimes (both healthy as well as diseased/disordered) (Markram, 2012; Van Essen et al., 2013; LeDoux, 1998). Ultimately, this will enable the improvement of people's quality of life.

Fortunately, each year, we get new insights and understanding about life-changing neurological diseases. These advances made in understanding neural systems that provide adequate treatment for these diseases have been mostly achieved with the help of technology that can measure and record neural activity (Fairclough and Lotte, 2020). Scientists and researchers use these measurements of the brain's activity to create models of the brain.

There are different methods to perform analysis and design of neural dynamical systems. One useful tool in modeling is dynamical network systems (Bassett and Sporns, 2017). For example, (Presigny and Fallani, 2021) provides an overview of the recent advances in modeling the multi-scale behavior of the brain using dynamical networks. These models have allowed researchers to draw conclusions regarding the brain's topology and func-

tion. While many studies have made use of linear dynamical system models (Ashourvan et al., 2020; Li et al., 2017; Pequito et al., 2017), these models are unable to capture the nonlinear and non-Markovian behavior exhibited in the brain (Zhang and Chen, 2012; West, 2016; Shlesinger et al., 1993). On the other hand, several studies make use of more complex nonlinear models; however, these models are not easy to interpret and explain in the context of brain dynamics (West et al., 2015; Bonilla et al., 2007).

Fractional-order dynamical systems originated in physics and economics and quickly found their way into engineering applications. Their appeal is mainly due to their representation as a compact spatiotemporal dynamical system with two easy-to-interpret sets of parameters, namely the *fractional-order exponents* and the *spatial coupling*. The fractional-order exponents capture the long-range memory in the dynamics of each state variable of the system and the spatial matrix represents the spatial coupling between different state variables, the latter being described by a matrix.

Fractional-order systems provide an efficient way to model many different systems (Valério et al., 2013; West, 2014; Kilbas et al., 2006; Baleanu et al., 2012; Podlubny, 1998; Sabatier et al., 2007; Xue and Bogdan, 2017; Lundstrom et al., 2008; Werner, 2010; Turcott and Teich, 1996; Thurner et al., 2003; Teich et al., 1997; Chen et al., 2010; Petráš, 2011). For example, fractional-order systems have been used in domains as disparate as biological networks (West et al., 2016), cyber-physical systems (Xue et al., 2016b), nanotechnology (Baleanu et al., 2010), finance (Scalas et al., 2000), quantum mechanics (Shahin et al., 2009), phasor measurement unit (PMU) data in the power grid (Shalalfeh et al., 2020), and networked control systems (Cao et al., 2009; Chen, 2010; Ren and Cao, 2011), to mention a few.

In this brief survey, we focus our attention on neural behavior, which can be accurately represented by fractional-order systems (Baleanu et al., 2011; West et al., 2016; Moon, 2008; Lundstrom et al., 2008; Werner, 2010; Thurner et al., 2003; Teich et al., 1997). Fractional-order systems have also been explored in the context of neurophysiological networks constructed from electroencephalographic (EEG), electrocorticographic (ECoG), or blood-oxygen-level-dependent (BOLD) data (Chatterjee et al., 2020; Magin, 2006).

Furthermore, we provide an overview of the work that has been done on controlling, estimating, and predicting neural dynamical systems modeled using fractional-order dynamics both in the continuous-time and discrete-time domains, towards the next generation of CNS. Specifically, the focus of our brief survey is threefold:

- Control: We review different methods of controlling fractional-order systems, including a few previously presented in (Efe, 2011). The work in (Birs et al., 2019) presents a survey of recent advances in fractional order control for time delay systems, and the works in (Matušu, 2011; Chen et al., 2009) provide overviews of the application of fractional calculus to control theory. In this paper, we review proportional-integral control, sliding mode control, backstepping control, adaptive control, optimal control, and model predictive control for fractional-order systems. Control of fractional-order systems is important to study so as to develop methods and therapies to mitigate and potentially eliminate diseases in the brain.
- System Identification: We focus on how to estimate the parameters of fractional-order systems from brain measurements, such as electroencephalography (EEG) and electrocorticography (ECoG), which is a necessary step in understanding the intricacies of the brain. Extensive attention has been paid to estimating the parameters of fractional-order systems, as evidenced in the following comprehensive works: (Ljung, 1999) and (Söderström and Stoica, 1989).
- Estimation: We discuss the methods for estimating and predicting the state of fractional-order systems (Sabatier et al., 2012; Sierociuk and Dzieliński, 2006; Safarinejadian et al., 2018, 2016; Miljković et al., 2017; Najar et al., 2009; Chatterjee and Pequito, 2019). This problem is important in anticipating and mitigating irregular brain behavior such as an oncoming seizure. (Chatterjee et al., 2021) proposed the design of a minimum-energy estimation framework for discrete-time fractional-order networks, where they assume that the state and output equations are affected by an additive disturbance and noise, respectively, that is considered to be deterministic, bounded, and unknown. First proposed by Mortensen (Mortensen, 1968), and later refined by Hijab (Hijab, 1980), minimum-energy estimators produce an estimate of the system state that is the "most consistent" with the dynamics and the measurement updates of the system (Fleming, 1997; Willems, 2004; Buchstaller et al., 2020; Swerling, 1971; Bonnabel and Slotine, 2015; Fagnani and Willems, 1997; Krener, 2003; Aguiar and Hespanha, 2006; Hassani et al., 2009; Pequito et al., 2009; Alessandretti et al., 2011; Ha and Aguiar, 2018; Haring and Johansen, 2020).

In what follows, we overview some of the definitions of both continuous and discrete fractional-order dynamics, towards assessing and designing different aspects of modeling, analysis, and control of the aforementioned. We start by introducing the fractional-order system in continuous-time (Kilbas and Trujillo, 2001, 2002).

1.1. Continuous-time fractional order systems

Riemann-Liouville and Caputo proposed the two popular (and equivalent) definitions of fractional order differintegration. Caputo's definition is the one widely used in control systems engineering, and it is the following:

$$\Delta^{\alpha}\sigma(t) = \frac{1}{\Gamma(m-\alpha)} \int_0^t \frac{\Delta^m \sigma(\tau)}{(t-\tau)^{\alpha+1-m}} d\tau, \tag{1}$$

where $\alpha \in \mathbb{R}^+$ is the differentiation order (Baleanu et al., 2012). Given the definition in (1), let $m \in \mathbb{Z}$ with $m-1 < \alpha < m$. For an m satisfying the previous relation, the α order derivative of a function of time, $\sigma(t)$, has the following Laplace transform:

$$\int_0^\infty e^{-st} \Delta^\alpha \sigma(t) \, dt = s^\alpha S(s) - \sum_{k=0}^{m-1} s^{\alpha-k-1} D^k \sigma(0), \tag{2}$$

where $\Gamma(\alpha) = \int_0^t e^{-t}t^{\alpha-1} dt$ is the Gamma function and $S(s) = \int_0^\infty e^{-st}\sigma(t) dt$.

If a system is, initially, in a resting state (i.e., the initial conditions are zero), then the operator Δ^{α} acting in the time domain has a counterpart s^{α} in the s-domain. In this case, we can describe the transfer function of a system by a fractional order differential equation

$$(a_n \Delta^{\alpha_n} + a_{n-1} \Delta^{\alpha_{n-1}} + \dots + a_1 \Delta^{\alpha_1} + a_0) y(t)$$

$$= (b_m \Delta^{\beta_m} + b_{m-1} \Delta^{\beta_{m-1}} + \dots + b_1 \Delta^{\beta_1} + b_0) u(t),$$
(3)

which we can obtain as

$$\frac{Y(s)}{U(s)} = \frac{a_n s^{\alpha_n} + a_{n-1} s^{\alpha_{n-1}} + \dots + a_1 s^{\alpha_1} + a_0}{b_m s^{\beta_m} + b_{m-1} s^{\beta_{m-1}} + \dots + b_1 s^{\beta_1} + b_0},\tag{4}$$

where $a_k, b_k \in \mathbb{R}$ and $\alpha_k, \beta_k \in \mathbb{R}^+$.

Therefore, we can write an affine and fractional-order nonlinear system as

$$\Delta^{\alpha} x(t) = \mathbf{f}(x(t)) + \mathbf{g}(x(t))u(t) \tag{5}$$

where u is the control input, and \mathbf{f} and $\mathbf{g} \neq 0$ are the vector functions of the system-state x(t). If the system is linear, then we can describe its state-space representation as

$$\Delta^{\alpha} x(t) = Ax(t) + Bu(t), \quad x(t) \in \mathbb{R}^{n}$$

$$y(t) = Cx(t) + Du(t).$$
 (6)

The transfer function characterizing the relation between Y(s) and U(s), and the Laplace transforms of the output and input, respectively, is as given as

$$H(s) = C (s^{\alpha}I - A)^{-1} B + D.$$
 (7)

Therefore, we have the following solution for the homogeneous case (u(t) = 0)

$$x(t) = E_{\alpha} \left(A t^{\alpha} \right) x(0) = \Phi(t) x(0), \tag{8}$$

where $E_{\alpha}(At^{\alpha})$ is the *Mittag-Leffler function* (Oldham and Spanier, 1974) defined as

$$\Phi(t) \equiv E_{\alpha} (At^{\alpha}) = \sum_{k=0}^{\infty} \left(\frac{(At^{\alpha})^{k}}{\Gamma(1+\alpha k)} \right).$$

Therefore, we can write the solution of the fractional state equation and the output equation in (6) as

$$y(t) = C\Phi(t - t_0) x(t_0) + C \int_0^t \Phi(t - \tau) Bu(\tau) d\tau + Du(t).$$

Despite the fact that real-world systems have continuous-time signals in nature, in reality, we measure and control these systems using digitized technologies, which motivates the study of discrete-time fractional-order systems (Caponetto, 2010; Goodrich and Peterson, 2015; Mahmoud, 2012). Subsequently, we now introduce the discrete-time description of the fractional-order dynamics.

1.2. Discrete-time fractional-order systems

In what follows next, we briefly introduce linear discrete-time fractional-order system models. A discrete-time linear fractional-order system model is described as follows:

$$\Delta^{\alpha}x[k+1] = Ax[k] + Bu[k] + w[k], \tag{9}$$

where x[k] is the state for time step $k \in \mathbb{N}$, $A \in \mathbb{R}^{n \times n}$ is the state coupling matrix and $\alpha \in (\mathbb{R}^n)^+$ is the vector of fractional-order coefficients. The signal $u[k] \in \mathbb{R}^{n_u}$ denotes the input corresponding to the actuation signal and the matrix $B \in \mathbb{R}^{n \times n_u}$ is the input matrix that scales the actuation signal. The term w[k] denotes the process noise or additive disturbance, whose stochastic characterization (or the lack thereof) will be clear from the context in which these systems are being used. These models are similar to classical discrete-time linear time-invariant system models with the exception of the inclusion of the (Grünwald-Letnikov) fractional derivative, whose expansion and discretization for the *i*-th state, $1 \le i \le n$, can be expressed as

$$\Delta^{\alpha_i} x_i[k] = \sum_{i=0}^k \psi(\alpha_i, j) x_i[k-j], \tag{10}$$

where α_i is the fractional-order coefficient corresponding to the state i and

$$\psi(\alpha_i, j) = \frac{\Gamma(j - \alpha_i)}{\Gamma(-\alpha_i)\Gamma(j + 1)},\tag{11}$$

with $\Gamma(\cdot)$ being the gamma function defined by $\Gamma(z) = \int_0^\infty s^{z-1}e^{-s} \, \mathrm{d}s$ for all complex numbers z with positive real part, $\Re(z) > 0$ (Vinagre et al., 2000; Dzielinski and Sierociuk, 2005). Simply put, larger values of the fractional-order coefficients imply a lower dependency on the previous data from that state (i.e., a faster decay of the weights used as linear combination of previous data).

We now review some essential theory for fractional-order systems, including an approximation of (9) with u[k] = 0 for all $k \in \mathbb{N}$ as an LTI system.

Using the expansion of the Grünwald-Letnikov derivative in (10), we have

$$\Delta^{\alpha}x[k] = \begin{bmatrix} \Delta^{\alpha_1}x_1[k] \\ \vdots \\ \Delta^{\alpha_n}x_n[k] \end{bmatrix} = \begin{bmatrix} \sum_{j=0}^k \psi(\alpha_1, j)x_1[k-j] \\ \vdots \\ \sum_{j=0}^k \psi(\alpha_n, j)x_n[k-j] \end{bmatrix}$$

$$= \sum_{j=0}^k \underbrace{\begin{bmatrix} \alpha_1 & \dots & 0 \\ \vdots & \ddots & \vdots \\ 0 & \dots & \alpha_n \end{bmatrix}}_{D(\alpha,j)} \begin{bmatrix} x_1[k-j] \\ \vdots \\ x_n[k-j] \end{bmatrix}$$

$$= \sum_{j=0}^k D(\alpha, j)x[k-j]. \tag{12}$$

The above formulation distinctly highlights one of the main peculiarities of DT-FODS in that the fractional derivative $\Delta^{\alpha}x[k]$ is a weighted linear combination of not just the previous state but of every single state up to the current one, with the weights given by (11) following a power-law decay.

Plugging (12) into the DT-FODS formulation (9) with u[k] = 0 for all $k \in \mathbb{N}$, we have

$$\sum_{j=0}^{k+1} D(\alpha, j) x[k+1-j] = Ax[k] + w[k], \tag{13}$$

or, equivalently,

$$D(\alpha, 0)x[k+1] = -\sum_{j=1}^{k+1} D(\alpha, j)x[k+1-j] + Ax[k] + w[k], \qquad (14)$$

which leads to

$$x[k+1] = -\sum_{i=0}^{k} D(\alpha, j+1)x[k-j] + Ax[k] + w[k],$$
 (15)

since $D(\alpha, 0) = I_n$, where I_n is the $n \times n$ identity matrix. Alternatively, (15) can be written as

$$x[k+1] = \sum_{j=0}^{k} A_j x[k-j] + w[k]$$

$$x[0] = x_0,$$
(16)

where

$$A_j = \begin{cases} A - \operatorname{diag}(\alpha_1, \dots, \alpha_n) & \text{if } j = 0 \\ -D(\alpha, j+1) & \text{if } j \ge 1 \end{cases}$$
 (17)

1.3. Paper organization

Section 2 presents the results on the stability of fractional-order sys-Section 3 provides a summary of the work on controllability and observability of fractional-order systems. Section 4 summarizes the work on proportional-integral-derivative controllers for fractional-order dynamical systems. Section 5 reviews sliding mode control for fractional-order systems. Section 6 outlines the procedure for constructing a backstepping controller for fractional-order systems. Section 7 summarizes adaptive control for fractional-order systems. Section 8 discusses the methods for performing system identification on fractional-order systems. Section 9 overviews the techniques for state estimation of fractional-order systems, including the method known as minimum-energy state estimation. Section 10 presents fractional optimal control for continuous-time fractional-order systems. Section 11 gives a background on model predictive control for fractional-order systems. Section 12 summarizes simulation results pertaining to system identification, state estimation, and closed-loop control of fractional cyber-neural systems. Finally, section 13 presents possible directions for future research.

2. Stability

Stability can be described as the behavior of the state of a system after a reasonable amount of time. While there are different notions of stability, in affect, a system is stable if the behavior of the system is bounded. The prior literature describes conditions for continuous-time fractional-order systems (Benzaouia et al., 2014; Li et al., 2009; Monje et al., 2010) and for single-input single-output continuous-time commensurate systems (i.e., systems with equal fractional exponents across state variables) (Dastjerdi et al., 2019). (Li et al., 2010) provides the generalized Mittag-Leffler stability conditions of continuous-time fractional-order systems using the Lyapunov direct method. In what follows, we summarize the stability conditions for continuous-time commensurate fractional-order systems. Let $\sigma(A) = \{\lambda_1, \ldots, \lambda_n\}$ be the spectrum (set of eigenvalues) of A. We say that the commensurate system in (6) is stable if

$$\arg(\lambda_i) > \alpha \frac{\pi}{2}, \quad \text{for all } i = 1, \dots, n,$$
 (18)

where $\arg(z)$, in the complex plane, is the 2D polar angle φ from the positive real axis to the vector representing z, and $0 < \alpha < 2$ (Rivero et al., 2013). In the case of the transfer function in (7), we have that $\sigma(A)$ corresponds to the poles of the system, and the previous stability condition of (18) also applies. Notice that, in the integer order case ($\alpha = 1$), the stability condition of (18) describes the open left half s-plane. For a more detailed discussion on the stability of continuous-time systems, we refer the reader to (Matignon, 1996; Chen et al., 2005; Ortigueira, 2000).

For discrete-time fractional-order systems, the authors of (Dzieliński and Sierociuk, 2008) leverage an infinite dimensional representation of truncated discrete-time fractional-order systems (i.e., with finite memory) to give conservative sufficient conditions for stability. While the work in (Busłowicz and Ruszewski, 2013) does provide necessary and sufficient conditions for practical and asymptotic stability of discrete-time fractional-order systems, they only consider commensurate-order systems (i.e., α is the same for all state variables). Recent work has introduced stability conditions for multivariate discrete-time fractional-order systems with arbitrary fractional exponents and leverages these conditions to study the stability of a real-world EEG cognitive motor data set modeled as a discrete-time fractional-order system and to provide evidence of its relevance in the context of cognitive motor control (Reed et al., 2021).

That said, a simple to state necessary and sufficient condition like (18) for non-commensurate both continuous and discrete-time systems is still missing. This limits the capacity to assess the stability of such systems and their applicability in the context of neural systems and possibly some neurological diseases such as epilepsy.

3. Controllability and observability

Controllability is a prerequisite in the ability to manipulate a system to any desired state in a finite amount of time. On the other hand, observability is necessary to obtain a complete picture of the system on the whole. For continuous-time systems, (Matignon and d'Andréa Novel, 1996) gives results on the controllability and observability of finite-dimensional continuous-time fractional-order systems. (Balachandran et al., 2013) gives a comprehensive overview of the conditions for controllability and observability of continuous-time linear fractional-order systems. Similarly, (Guermah et al., 2008) provides these results for discrete-time linear fractional-order systems. The work

in (Mozyrska and Pawłuszewicz, 2012) derives the conditions for controllability and observability of finite memory discrete-time fractional-order systems.

Previous work has examined the design of controllable networks exhibiting discrete-time linear fractional-order dynamics using energy-based methods (Kyriakis et al., 2020) and by maximizing the rank of the controllability matrix through a greedy algorithm (Cao et al., 2019). Similarly, there has been work in selecting the minimal number of EEG sensors to achieve observability for discrete-time fractional-order systems (Gupta et al., 2018a; Xue et al., 2016a; Tzoumas et al., 2018; Pequito et al., 2015).

A system is controllable if there exists a control input such that the final state can be driven to zero in a finite amount of time. In particular, for continuous-time linear fractional-order systems modeled by (6), the system is controllable on $[t_0, t_1]$ if for every pair of vectors $x(t_0), x(t_1) \in \mathbb{R}^n$, there is a control $u(t) \in L^2([t_0, t_1], \mathbb{R}^m)$ such that the solution x(t) of (6) which satisfies $x(t_0) = x_0$ also satisfies $x(t_1) = x_1$, where $L^2([t_0, t_1], \mathbb{R}^m)$ is the space of all square integrable \mathbb{R}^m valued measureable functions defined on $[t_0, t_1]$. Thus, we say that (6) is controllable on $[t_0, t_1]$ if and only if the controllability Gramian matrix

$$\int_{t_0}^{t_1} (t_1 - \tau)^{\alpha - 1} E_{\alpha, \alpha} (A(t_1 - \tau)^{\alpha}) B B^{\mathsf{T}} E_{\alpha, \alpha} (A^{\mathsf{T}} (t_1 - \tau)^{\alpha}) d\tau$$

is positive definite for some $t_1 > t_0$ (Theorem 3, (Balachandran et al., 2013)).

For discrete-time linear fractional-order system modeled by (9), the system is controllable if there exists a control sequence $\{\mathbf{u}[0], \dots, \mathbf{u}[T-1]\}$ such that $\mathbf{x}[T] = \mathbf{0}$ from any initial state $\mathbf{x}[0] \in \mathbb{R}^n$ in a finite time (Guermah et al., 2008). To present the conditions for controllability and observability for discrete-time fractional-order systems, we first start by noticing that the discrete-time linear fractional-order system (9) can be re-written as (Gupta et al., 2018a, Lemma 2):

$$x[k] = G_k x[0], (19)$$

where

$$G_k = \begin{cases} I_n, & k = 0\\ \sum_{j=0}^{k-1} A_j G_{k-1-j}, & k \ge 1 \end{cases}$$
 (20)

with $A_0 = A - D(\alpha, 1)$, $A_j = -D(\alpha, j + 1)$, for $j \ge 1$, and

$$D(\alpha, j) = \begin{bmatrix} \psi(\alpha_1, j) & 0 & \dots & 0 \\ 0 & \psi(\alpha_2, j) & \dots & 0 \\ 0 & \vdots & \ddots & 0 \\ 0 & 0 & \dots & \psi(\alpha_n, j) \end{bmatrix}.$$
 (21)

The linear discrete-time fractional-order system modeled by (9) is controllable if and only if there exists a finite time K such that $\operatorname{rank}(W_c(0,K)) = n$, where $W_c(0,K) = G_K^{-1} \sum_{j=0}^{K-1} G_j B B^{\mathsf{T}} G_j^{\mathsf{T}} G_K^{\mathsf{T}}$ (Guermah et al., 2008, Theorem 4). Furthermore, an input sequence $[\mathbf{u}^{\mathsf{T}}[K-1], \mathbf{u}^{\mathsf{T}}[K-2], \dots \mathbf{u}^{\mathsf{T}}[0]]^{\mathsf{T}}$ that transfers $\mathbf{x}[0] \neq 0$ to $\mathbf{x}[K] = 0$ is given by

$$\begin{bmatrix} \mathbf{u}[K-1] \\ \mathbf{u}[K-2] \\ \vdots \\ \mathbf{u}[0] \end{bmatrix} = -[G_0BG_1B\dots G_{K-1}B]^{\mathsf{T}}G_K^{-\mathsf{T}}W_c^{-1}(0,K)\mathbf{x}[0]. \tag{22}$$

Similarly, a system is observable if and only if the initial state $\mathbf{x}[0]$ can be uniquely determined from the knowledge of the control input and observations. For continuous-time systems, the system is observable on an interval $[t_0, t_1]$ if y(t) = Cx(t) = 0 for $t \in [t_0, t_1]$ implies x(t) = 0 for $[t_0, t_1]$. Hence, the system in (6) is observable on $[t_0, t_1]$ if an only if the observability Gramian matrix $W = \int_{t_0}^{t_1} E_{\alpha}(A^{\mathsf{T}}(t-t_0)^{\alpha})C^{\mathsf{T}}CE_{\alpha}(A(t-t_0)^{\alpha}) dt$ is positive definite (Balachandran et al., 2013, Theorem 1).

For linear discrete-time fractional-order systems modeled by (9), the system is said to be observable if and only if there exists some K > 0 such that the initial state $\mathbf{x}[0]$ at time k = 0 can be uniquely determined from the knowledge of $\{\mathbf{u}[0], \ldots, \mathbf{u}[K-1]\}$ and $\{\mathbf{y}[0], \ldots, \mathbf{y}[K-1]\}$. Therefore, by Theorem 5 in (Guermah et al., 2008), the linear discrete-time fractional-order system is observable if and only if there exists a finite time K such that $\operatorname{rank}(\mathcal{O}_K) = n$, where $\mathcal{O}_K = \begin{bmatrix} CG_0, CG_1, \ldots, CG_{K-1} \end{bmatrix}^{\mathsf{T}}$ or, equivalently, $\operatorname{rank}(W_o(0,K)) = n$, where $W_o(0,K) = \sum_{j=0}^{K-1} G_j^{\mathsf{T}} C^{\mathsf{T}} C G_j$. Furthermore, the initial state at $\mathbf{x}[0]$ is given by

$$\mathbf{x}[0] = W_o^{-1}(0, K) \mathcal{O}_K^{\mathsf{T}}[\tilde{\mathcal{Y}}_K - \mathcal{M}_K \tilde{\mathcal{U}}_K], \tag{23}$$

where
$$\tilde{\mathcal{U}}_K = \left[\mathbf{u}^{\mathsf{T}}[0], \mathbf{u}^{\mathsf{T}}[1], \dots, \mathbf{u}^{\mathsf{T}}[K-1]\right], \ \tilde{\mathcal{Y}}_K = \left[\mathbf{y}^{\mathsf{T}}[0], \dots, \mathbf{y}^{\mathsf{T}}[K-1]\right]^{\mathsf{T}},$$
 and

$$\mathcal{M}_K = \begin{bmatrix} 0 & 0 & \dots & 0 & 0 \\ CG_0B & 0 & \dots & 0 & 0 \\ CG_1B & CG_0B & \dots & 0 & 0 \\ CG_2B & CG_1B & \dots & 0 & 0 \\ \vdots & \vdots & \ddots & \vdots & \vdots \\ CG_{K-2}B & CG_{K-3}B & \dots & CG_0B & 0 \end{bmatrix}.$$

4. Proportional-integral-derivative control

A proportional-integral-derivative controller (PID controller or three-term controller) is a control loop mechanism. It employs feedback and is commonly utilized in industrial control systems and a variety of other applications that need a continuously modulated control. A PID controller continuously computes an error value as the difference between the desired setpoint (SP) and a measured process variable (PV) and implements a correction based on proportional, integral, and derivative terms (P, I, and D, respectively).

A simple and practical example is the cruise control of a vehicle. For example, if only constant engine power is applied, a car ascending a hill would lose speed. In a situation like this, the controller's PID algorithm is responsible for restoring the measured speed to the desired cruise control speed. Moreover, the PID control increases the power output of the engine in a controlled manner, with minimal delay and overshoot.

The interpretability and comprehensibility of PID controllers make it a typical choice regarding peripherals that automatically tune the system's parameters without external intervention. The work in (Podlubny, 1999) provides the framework for fractional-order PID control, which we summarize next. We can define the fractional order version of PID controllers using the following transfer function:

$$C(s) = k_p + \frac{k_i}{s^{\lambda}} + k_d s^{\mu}. \tag{24}$$

For $\lambda = 1$ and $\mu = 1$, we obtain the standard integer order setting with three degrees of freedom: k_p, k_i , and k_d . Notwithstanding, in (24), we have five parameters to determine, yielding five independent specifications that we can force to meet. If we place the controller in front of a G(s) in a unity feedback loop, then the first specification can be on phase margin as

it is tightly coupled with the robustness of the control system. The equations that define the phase margin are $20 \log |C(w_{qc})G(w_{qc})| = 0$ dB and $\arg (C(w_{gc})G(w_{gc})) = -\pi + \varphi_{pm}$, where w_{gc} is the gain crossover frequency and φ_{pm} the phase margin.

Subsequently, we may force a flat magnitude response |G(jw)C(jw)| around the gain crossover frequency. We can ensure this response, see (Monje et al., 2008), by setting the derivative $\frac{d}{dw}(\arg(C(jw)G(jw)))$ to zero when $w = w_{cg}$. Moreover, ensuring this constraint makes the closed-loop control system robust against variations in the gain of G(s).

Another specification supposes that a controller introduces the property of noise rejection in high frequencies. This property can be accomplished by fixing a critical frequency, w_h . If this frequency is exceeded, then the magnitude of the transfer function T = CG/(1 + CG) (corresponding to the complementary sensitivity function) is smaller than a preselected level.

Next, how can we ensure that a good output disturbance is not rejected? To address this, we can force an upper bound (M) on the sensitivity function's magnitude below a predefined frequency (w_s) . Hence, it follows that

$$20 \log |S(jw)|_{w \le w_s} = 20 \log \left| \frac{1}{1 + C(jw)G(jw)} \right|_{w < w_s} \le M \text{ dB.}$$

In the final step, to achieve a zero steady-state error, we need to design the controller C(s) with an integral component.

Notice that, although solving the necessary set of equations from the constraints above is one way to establish the parameters k_p , k_i , k_d , λ , and μ , this requires the prior knowledge of model order, dead time, poles and zeros. In the scenario where we do not have this prior knowledge, we may, alternatively, resort to *autotuning* (Monje et al., 2008; Chen et al., 2004).

5. Sliding mode control

In control systems, sliding mode control (SMC) is a nonlinear control method that adjusts the dynamics of a nonlinear system by applying a discontinuous control signal (a set-valued control signal). This control signal compels the system to "slide" along a cross-section of the system's normal behavior. In this case, the state-feedback control law is not a function continuous in time. Instead, it can switch between continuous structures based on the state space current position to achieve the desired behavior. There

are two stages in SMC: (i) the reaching phase, which is the phase that lasts until the hitting of a trajectory to the switching subspace; (ii) the sliding mode, which is the motion after the previous phase. A relevant property of stage (ii) is the robustness against disturbances and variations in the process parameters – i.e., the invariance property.

Now, we present a set of results regarding SMC for fractional order systems. Given the nth order fractional dynamic system in (5) and the following switching function

$$\sigma(t) = \Lambda \left(c(t) - r(t) \right), \tag{25}$$

where Λ is a parameter designed to make the sliding manifold defined by $\sigma=0$ to be a stable subspace, where the stability can be settled via (18). This entails that, despite the process being nonlinear, the nominal plant model is linear. If $0<\alpha<1$ and r is the vector of differentiable command signals, then the goal of the reaching law approach is to get $\Delta^{\alpha}\sigma(t)=-k\,\mathrm{sgn}(\sigma(t))$ for some k>0. When $\alpha=1$, it corresponds to $\dot{\sigma}(t)=-k\,\mathrm{sgn}(\sigma(t))$, which ensures $\sigma(t)\dot{\sigma}(t)<0$ whenever $\sigma\neq0$. This solution is the time derivative of the Lyapunov function $V=\frac{1}{2}\sigma(t)^2$, which physical meaning is to provide the sliding manifold an attractor such that, once the error vector gets trapped to it, the subsequent motion takes place in the proximity of the sliding hypersurface.

Next, we need to show that the aforementioned mechanism also works for non-integer differentiation order (Vinagre and Calderón, 2006). We start by differentiating $\Delta^{\alpha} \sigma(t) = -k \operatorname{sgn}(\sigma(t))$ at the order $-\alpha$

$$\Delta^1 \left(\Delta^{-\alpha} \left(\Delta^{\alpha} \sigma(t) \right) \right) = -k \Delta^1 \left(\Delta^{-\alpha} \operatorname{sgn}(\sigma(t)) \right)$$

and, next, differentiate at order unity to obtain $\dot{\sigma}(t)$

$$\dot{\sigma}(t) = -k\Delta^{1-\alpha}\operatorname{sgn}(\sigma(t)).$$

Because $0 < \alpha < 1$, it follows that $\operatorname{sgn}(\Delta^{1-\alpha}\operatorname{sgn}(\sigma(t))) = \operatorname{sgn}(\sigma(t))$. Forcing $\Delta^{\alpha}\sigma(t) = -k\operatorname{sgn}(\sigma(t))$ makes the locus described by $\sigma = 0$ a global attractor.

It is easy to check that choosing $\Delta^{\alpha}\sigma(t) = -k\operatorname{sgn}(\sigma(t)) - p\sigma(t)$ with p > 0 has the same effect on the reaching dynamics of that in the integer order design. Notice that with $p\sigma = p|\sigma(t)|\operatorname{sgn}(\sigma)$, the following relation holds between $\dot{\sigma}(t)$ and $\operatorname{sgn}(\sigma(t))$:

$$\begin{split} \dot{\sigma}(t) &= -k\Delta^{1-\alpha}\operatorname{sgn}(\sigma(t)) - p\Delta^{1-\alpha}(|\sigma(t)|\operatorname{sgn}(\sigma(t))) \\ &= -\Delta^{1-\alpha}((k+p|\sigma(t)|)\operatorname{sgn}(\sigma(t))). \end{split}$$

Notice that, since $\operatorname{sgn}(\Delta^{1-\alpha}\operatorname{sgn}(\sigma(t))) = \operatorname{sgn}(\sigma)$, the reaching dynamics governed by the above expression generates a stronger push from both sides of the switching manifold. This effect translates into the attraction strength of the switching manifold being higher, for any $\sigma(t)$ with $p \neq 0$, than for p = 0. Moreover, for a fixed $\sigma(t)$, larger values of p create larger values of $\dot{\sigma}(t)$, which leads to reaching quicker the place characterized by $\sigma = 0$. If we select the Lyapunov function $V(t) = \frac{1}{2}\sigma(t)^2$ and compute its α th order derivative, using the Leibniz's differentiation rule, we obtain

$$\Delta^{\alpha}V(t) = \sum_{k=0}^{\infty} \frac{\Gamma(1+\alpha)}{\Gamma(1+k)} \Gamma(1-k+\alpha) \Delta^{k}\sigma(t) \Delta^{\alpha-k}\sigma(t),$$

i.e., an expression with infinitely many terms. Therefore, we are not able to infer the attractiveness of $\sigma(t) = 0$, deduced from $\sigma(t)\Delta^{\alpha}\sigma(t) < 0$, or more specifically, from $\Delta^{\alpha}\sigma(t) = -k \operatorname{sgn}(\sigma(t)) - p\sigma(t)$.

Recalling definition (1), the following equality holds

$$\sigma(t)\Delta^{\alpha}\sigma(t) = \frac{\sigma(t)}{\Gamma(1-\alpha)} \int_0^t \frac{\Delta\sigma(\tau)}{(t-\tau)^{\alpha}} d\tau.$$

The previous relation imposes two possibilities to have that $\sigma(t)\Delta^{\alpha}\sigma(t) < 0$:

- (i) if $\sigma(t) > 0$, then $\Delta \sigma(t)$ (the first derivative of $\sigma(t)$) must be negative;
- (ii) if $\sigma(t) < 0$, then $\Delta \sigma(t)$ (the first derivative of $\sigma(t)$) must be positive.

In conclusion, an appropriately designed control law is sufficient for closed-loop stability, forcing $\sigma \Delta^{\alpha} \sigma(t) < 0$. Therefore, the stability requirement $\sigma(t)\dot{\sigma}(t) < 0$ (or $\sigma(t)\Delta\sigma(t) < 0$) of the integer order design is obtained naturally, whenever we impose $\sigma(t)\Delta^{\alpha} \sigma(t) < 0$.

In (Efe, 2011), the following is proposed. Compute α th order derivative of (25), which is

$$\Delta^{\alpha} \sigma(t) = \mathbf{\Lambda} \left(\Delta^{\alpha} x(t) - \Delta^{\alpha} r(t) \right) = \mathbf{\Lambda} \left(\mathbf{f}(x(t)) + \mathbf{g}(x(t)) u(t) - \Delta^{\alpha} r(t) \right).$$

Next, setting the previous expression equal to $-k \operatorname{sgn}(\sigma(t)) - p\sigma(t)$ and solving for u yields the following control signal:

$$u(t) = \frac{-\Lambda \mathbf{f}(x(t)) + \Lambda \Delta^{\alpha} r(t) - k \operatorname{sgn}(\sigma(t)) - p\sigma(t)}{\Lambda g(x(t))},$$
(26)

where we need to have that $\Lambda g(x(t)) \neq 0$. Having the encountered control law, deduced from a nominal model, an important question is what would be the response of the system, whenever the model in (5) is a nominal representation of a plant holding the uncertainties $\Delta \mathbf{f}(x(t))$ and $\Delta \mathbf{g}(x(t))$, such as the following

$$\Delta^{\alpha} x(t) = (\mathbf{f}(x(t)) + \Delta \mathbf{f}(x(t))) + (\mathbf{g}(x(t)) + \Delta \mathbf{g}(x(t)))u(t). \tag{27}$$

Combining (26) and (27) yields the following dynamics

$$\Delta^{\alpha} \sigma(t) = -\left(1 + \frac{\mathbf{\Lambda} \Delta \mathbf{g}(x(t))}{\mathbf{\Lambda} \mathbf{g}(x(t))}\right) (k \operatorname{sgn}(\sigma(t)) + p\sigma(t)) + \frac{\mathbf{\Lambda} \Delta \mathbf{g}(x(t))}{\mathbf{\Lambda} \mathbf{g}(x(t))} \mathbf{\Lambda} (\Delta^{\alpha} r(t) - \mathbf{f}(x(t))) + \mathbf{\Lambda} \Delta \mathbf{f}(x(t)).$$
(28)

Hence, we have the following properties:

- If there are no uncertainties, i.e., $\Delta \mathbf{f}(x(t)) = \Delta \mathbf{g}(x(t)) = 0$, then we have $\Delta^{\alpha} \sigma(t) = -k \operatorname{sgn}(\sigma(t)) p\sigma(t)$, being desired to observe the sliding regime, after hitting the sliding hypersurface;
- If $\Delta \mathbf{g}(x(t)) = 0$ and the columns of $\Delta \mathbf{f}(x(t))$ are in the range space of $\mathbf{g}(x(t))$, then $\Delta^{\alpha} \sigma(t) = -k \operatorname{sgn}(\sigma(t)) p\sigma + \mathbf{\Lambda} \Delta \mathbf{f}(x(t))$. This case further requires the hold of the condition in of $|A\Delta \mathbf{f}(x(t))| < k$ to ensure that $\sigma(t)\Delta^{\alpha} \sigma(t) < 0$;
- If the uncertainty terms are nonzero, then (28) is valid, which implies that the designer has to carefully set k and p to keep the attractiveness of the subspace defined by $\sigma(t) = 0$ The following two conditions are required to ensure that $\sigma(t)\Delta^{\alpha}\sigma(t) < 0$:

$$\left| \frac{\Lambda \Delta g(x(t))}{\Lambda g(x(t))} \right| < 1$$

$$\left(1 + \frac{\Lambda \Delta g(x(t))}{\Lambda g(x(t))} \right) k > \left| \frac{\Lambda \Delta g(x(t))}{\Lambda g(x(t))} \Lambda \left(\Delta^{\alpha} r(t) - f(x(t)) \right) + \Lambda \Delta f(x(t)) \right|.$$

The columns of $\Delta \mathbf{f}(x(t))$ and $\Delta \mathbf{g}(x(t))$ are assumed to be in the range space of $\mathbf{g}(x(t))$, i.e., the uncertainties are matched. If the previous condition is not satisfied, then the closed-loop performance will deteriorate.

Finally, notice that the first hitting to the switching subspace yields when $t = t_h$, where $t_h = (|\sigma(0)|\Gamma(\alpha+1)/k)^{1/\alpha}$.

6. Backstepping control

Backstepping is a technique developed in the 90s by Petar V. Kokotovic and others (Kokotovic, 1992; Lozano et al., 1992). The goal of this technique is to design stabilizing controls for a special class of nonlinear dynamical systems. These systems consist of subsystems that radiate out from an irreducible subsystem, which we can stabilize using some method. Due to its recursive structure, the designer can start the design process at the known-stable system and "back out" new controllers that progressively stabilize each outer subsystem. The process of stabilization stops when the final external control is achieved. In other words, backstepping is based on the definition of a set of intermediate variables and the process of ensuring the negativity of Lyapunov functions that are combined to form a common control Lyapunov function for the overall system.

In fact, we can use the backstepping technique in a particular but wide class of systems. Consider the following system

$$x_1^{(\alpha_1)}(t) = x_2(t) x_2^{(\alpha_2)}(t) = \mathbf{f}(x_1(t), x_2(t)) + \mathbf{g}(x_1(t), x_2(t)) u(t),$$
(29)

where x_1 and x_2 are the state variables, $0 < \alpha_1, \alpha_2 < 1$ are positive fractional differentiation orders, \mathbf{f} and \mathbf{g} are known and smooth functions of the state variables such that $\mathbf{g}(x_1(t), x_2(t)) \neq 0$. Additionally, consider the intermediate variables of backstepping design:

$$z_1(t) = x_1(t) - r_1(t) - A_1(t)$$

$$z_2(t) = x_2(t) - r_2(t) - A_2(t),$$

where $A_1(t) = 0$ and $r_1^{(\alpha_1)}(t) = r_2(t)$.

Subsequently, consider the Lyapunov function with variable of interest z

$$V(t) = \frac{1}{2}z^2(t).$$

Now, from Section 5, we have that $z(t)z^{(\alpha)}(t)$ ensures $z(t)\dot{z}(t) < 0$, for any $0 < \alpha < 1$. That said, we formulate the backstepping control technique for the plant described by (29), by checking recurrently the quantities $z_1(t)z_1^{(\alpha_1)}(t)$ and $z_1(t)z_1^{(\alpha_1)}(t) + z_2(t)z_2^{(\alpha_2)}(t)$ as the following steps:

1. Check $z_1(t)z_1^{(\alpha_1)}(t)$:

$$z_1(t)z_1^{(\alpha_1)}(t) = z_1(t) \left(x_1^{(\alpha_1)}(t) - r_1^{(\alpha_1)}(t) \right)$$

$$= z_1(t) \left(x_2(t) - r_2(t) \right)$$

$$= z_1(t) \left(z_2(t) + r_2(t) + A_2(t) - r_2(t) \right)$$

$$= z_1(t) \left(z_2(t) + A_2(t) \right)$$

2. Choose $A_2(t) = -k_1 z_1(t)$, with $k_1 > 0$, this would entail that

$$z_1(t)z_1^{(\beta_1)}(t) = -k_1z_1^2(t) + z_1(t)z_2(t)$$

3. Check $z_1(t)z_1^{(\alpha_1)}(t) + z_2(t)z_2^{(\alpha_2)}(t)$:

$$\begin{split} z_1(t)z_1^{(\alpha_1)}(t) + z_2(t)z_2^{(\alpha_2)}(t) \\ &= -k_1 z_1^2(t) + z_1(t) z_2(t) + z_2 \left(x_2^{(\alpha_2)}(t) - r_2^{(\alpha_2)}(t) - A_2^{(\alpha_2)}(t) \right) \\ &= -k_1 z_1^2(t) + z_2(t) \left(x_2^{(\alpha_2)}(t) - r_2^{(\alpha_2)}(t) - A_2^{(\alpha_2)}(t) + z_1(t) \right) \\ &= -k_1 z_1^2(t) + z_2(t) \left(\mathbf{f} \left(x_1(t), x_2(t) \right) + \mathbf{g} \left(x_1(t), x_2(t) \right) u(t) \right. \\ &\left. - r_2^{(\alpha_2)}(t) - A_2^{(\alpha_2)}(t) + z_1(t) \right) \end{split}$$

4. Force $z_1(t)z_1^{(\alpha_1)}(t) + z_2(t)z_2^{(\alpha_2)}(t) = -k_1z_1^2(t) - k_2z_2^2(t)$, with $k_2 > 0$, which implies that

$$\mathbf{f}(x_1(t), x_2(t)) + \mathbf{g}(x_1(t), x_2(t))u(t) - r_2^{(\alpha_2)}(t) - A_2^{(\alpha_2)}(t) + z_1(t) = -k_2 z_2(t)$$

5. Obtain for u:

$$u(t) = -\frac{\mathbf{f}(x_1(t), x_2(t)) - r_2^{(\alpha_2)}(t) + k_1(t)z_1^{(\alpha_2)}(t) + z_1(t) + k_2z_2(t)}{\mathbf{g}(x_1(t), x_2(t))}$$

In fact, we can generalize the aforementioned procedure for systems of higher order of the form

$$x_i^{(\alpha_i)}(t) = x_{i+1}(t), \text{ for } i = 1, \dots, q-1$$

 $x_q^{(\alpha_q)}(t) = \mathbf{f}(x_1(t), \dots, x_q(t)) + \mathbf{g}(x_1(t), \dots, x_q(t)) u(t),$

where the resulting control law, in this case, is

$$u(t) = -\frac{\mathbf{f}(x_1(t), \dots, x_q(t)) - r_q^{(\alpha_q)}(t) - A_q^{(\alpha_q)}(t) + z_{q-1}(t) + k_q z_q(t)}{\mathbf{g}(x_1(t), \dots, x_q(t))}, \quad (30)$$

where $k_j > 0$, for j = 1, ..., q, and A_i is given by the following recurrence relation:

$$A_1(t) = 0,$$
 $z_0(t) = 0$
 $A_{i+1}(t) = -k_i z_i(t) + A_i^{(\alpha_i)}(t) - z_{i-1}(t),$ for $i = 1, \dots, q-1$.

Now, the result of applying the control law in detailed in (30) is

$$\sum_{i=1}^{q} z_i(t) z_i^{(\alpha_i)}(t) = -\sum_{i=1}^{q} k_i z_i^2(t).$$
 (31)

Finally, to ensure the negativeness of the right-hand side of (31) is the same as to ensure the negativity of $\sum_{i=1}^{q} z_i(t)\dot{z}_i(t)$, and the trajectories in the coordinate system spanned by $z_1(t), \ldots, z_q(t)$ will converge the origin point.

7. Adaptive control

Adaptive control is the control method used by a controller that must adapt to a controlled system with parameters that either vary over time or are initially uncertain. Therefore, it is desirable to have a control law that adapts itself to the changing conditions. In other words, adaptive control is a good alternative for industrial applications where the process parameters change, and the controller needs to automatically adapt itself to the new operating conditions. This aptitude is called adaptiveness. Here, the role of fractional calculus is to design noninteger order adaptation laws or select reference models of noninteger order (Monje et al., 2010).

A broadly adopted adaptive control structure is the so-called *model reference adaptive control* (MRAC) – see Fig. 1. This control strategy is grounded on the assumption that the changes in the process parameters are slower than other changes in the closed-loop system. Hence, the parameter adjustment mechanism employs the difference between the model output $(y_m(t))$ and the process response (y(t)) and uses the gradient rule to adjust the parameters of the control law:

$$\Delta^{\alpha}\phi(t) = -\eta \frac{\partial J(t)}{\partial \phi(t)} = -\eta e(t) \frac{\partial e(t)}{\partial \phi(t)},\tag{32}$$

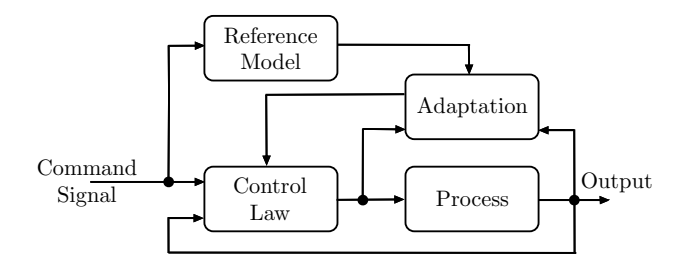


Figure 1: Diagram of the MRAC control scheme.

where $\phi(t)$ is a generic parameter of the control law, $e(t) = y(t) - y_m(t)$ is the instantaneous model following error, and $J(t) = \frac{e^2(t)}{2}$ is the instantaneous performance measure.

It is worth noticing that, when $\alpha=1$ in (32), we get the traditional update laws. Additionally, we refer to (Monje et al., 2010) for a detailed example considering a fractional order reference model, where stability is also sought. Furthermore, the benefit of utilizing a fractional order setting in MRAC is to achieve a shorter transient regime compared to the classical case. This property might be critical in applications demanding a high-speed response.

8. System identification

The problem of learning the fractional-order dynamical systems' parameters, i.e., the fractional coefficients and the spatiotemporal matrix, is challenging. Specifically, the determination of the maximum-likelihood poses limitations due to the nonlinearity of the objective. Notwithstanding, some approaches were successfully developed in (Gupta et al., 2018a,b, 2019), where an approximate solution is based on a variant of the expectation-maximization algorithm. Nonetheless, such approaches do not enable a finite-time assessment of the uncertainty associated with the parameters, that play a key role in the context of CNS.

Therefore, in what follows, we a recent approach relies on a bilevel iterative bisection scheme (Chatterjee and Pequito, 2021) to perform identification of the spatial and temporal parameters of a linear discrete-time fractional-

order system. First, consider

$$\tilde{x}[k] = \begin{bmatrix} x[k] \\ x[k-1] \\ \vdots \\ x[k-p+1] \end{bmatrix}$$
(33)

as the *augmented* state vector and assuming that the system is *causal*, i.e., the state and disturbances are all considered to be zero before the initial time (i.e., x[k] = 0 and w[k] = 0 for all k < 0), we have

$$\tilde{x}[k+1] = \underbrace{\begin{bmatrix} A_0 & \dots & A_{p-2} & A_{p-1} \\ I & \dots & 0 & 0 \\ \vdots & \ddots & \vdots & \vdots \\ 0 & \dots & I & 0 \end{bmatrix}}_{\tilde{A}} \tilde{x}[k] + \underbrace{\begin{bmatrix} I \\ 0 \\ \vdots \\ 0 \end{bmatrix}}_{\tilde{B}^w} w[k]$$

$$= \tilde{A}\tilde{x}[k] + \tilde{B}^w w[k], \tag{34}$$

for all $k \geq 0$. Note that (34) is an LTI system model, which we refer to as the *p-augmented LTI approximation* of (9).

Having established the p-augmented LTI approximation of a DT-FODS in (34), we can consider the two-level iterative bisection-like approach to identify the spatial and temporal parameters of the DT-FODS in (9). In particular, we start by noting the fact that for the Grünwald-Letnikov definition of the fractional derivative provided in (10), $\alpha_i = 1$ and $\alpha_i = -1$ can be interpreted, respectively, to be the discretized version of the derivative and the integral for $1 \le i \le n$, as defined in the sense of ordinary calculus.

To proceed with a bisection-like approach to identify $\{\alpha_i\}_{i=1}^n$ and \tilde{A} , we first fix the endpoints of the search space for α_i to be $\underline{\alpha_i} = -1$ and $\overline{\alpha_i} = 1$ for $1 \leq i \leq n$. We also calculate the value of $\alpha_{c,i} = (\underline{\alpha_i} + \overline{\alpha_i})/2$. Now, given the values of $\underline{\alpha_i}$, $\overline{\alpha_i}$, and $\alpha_{c,i}$, we calculate, using the ordinary least squares (OLS) technique described in detail below, the row vectors $\underline{\tilde{a}_i}$, $\overline{\tilde{a}_i}$, and $\tilde{a}_{c,i}$, respectively, that guide the evolution of the states in the p-augmented LTI approximation

$$\tilde{x}_i[k+1] = \tilde{a}_i \tilde{x}_i[k] + \tilde{b}_i^w w_i[k], \tag{35}$$

where $\tilde{a}_i = \underline{\tilde{a}}_i$ when $\alpha_i = \underline{\alpha}_i$, $\tilde{a}_i = \overline{\tilde{a}}_i$ when $\alpha_i = \overline{\alpha}_i$, and $\tilde{a}_i = \tilde{a}_{c,i}$ when $\alpha_i = \alpha_{c,i}$ with \tilde{b}_i^w being obtained by extracting the *i*-th row of \tilde{B}^w for $1 \le i \le n$.

Next, we propagate the dynamics according to the obtained values of the parameters \tilde{a}_i and calculate the mean squared error (MSE) between the states obtained as a result of the estimated \tilde{a}_i 's and the observed states. If the MSE is smaller corresponding to the $\underline{\alpha}_i$ case, then we set $\overline{\alpha}_i = \alpha_{c,i}$. If the MSE is smaller corresponding to the $\overline{\alpha}_i$ case, then we set $\underline{\alpha}_i = \alpha_{c,i}$. This approach is repeated until $|\overline{\alpha}_i - \underline{\alpha}_i|$ does not exceed a certain pre-specified tolerance ε . Algorithm 1 summarizes the procedure of determining the spatial and temporal components of a DT-FODS using the two-level iterative bisection-like approach that we have outlined above.

Therefore, for the estimation of the temporal components of a DT-FODS, we specify the iteration complexity of the bisection-like process and then, we investigate the finite-sample complexity of computing the spatial parameters using a least squares approach.

First, numerical and experimental evidence suggests that the computation of the temporal parameters of a DT-FODS, using, e.g., a wavelet-like technique described in (Flandrin, 1992), does not directly depend on the number of samples or observations used for the aforementioned estimation procedure. Empirical evidence suggests that a small number of samples (usually 30 to 100) suffice in order to compute $\{\alpha_i\}_{i=1}^n$. Furthermore, we can certify the iteration complexity of the bisection method to find the spatial and temporal parameters of a DT-FODS. Specifically, the bisection-based technique detailed above to find the temporal components of a DT-FODS is minmax optimal and the number ν of iterations needed in order to achieve a certain specified tolerance ε when this technique is used is bounded above by

$$\nu \le \left\lceil \log_2\left(\frac{2}{\varepsilon}\right) \right\rceil. \tag{36}$$

Secondly, we can now delve into the problem of identifying the spatial parameters using a least squares-like approach and its finite-time guarantees. We start with the p-augmented LTI model of (34), i.e.,

$$\tilde{x}[k+1] = \tilde{A}\tilde{x}[k] + \tilde{B}^w w[k]. \tag{37}$$

The OLS method then outputs the matrix $\underline{\tilde{A}}[K]$ as the solution of the following optimization problem

$$\underline{\tilde{A}}[K] := \underset{\tilde{A} \in \mathbb{R}^{d \times d}}{\operatorname{argmin}} \sum_{k=1}^{K} \frac{1}{2} \left\| \tilde{x}[k+1] - \tilde{A}\tilde{x}[k] \right\|_{2}^{2}, \tag{38}$$

Algorithm 1 Learning the parameters of a DT-FODS

- 1: **for** i = 1 to n **do**
- 2: Initialize $\alpha_i = -1$, $\overline{\alpha_i} = 1$, and tolerance ε .
- 3: Calculate $\alpha_{c,i} = (\alpha_i + \overline{\alpha_i})/2$.
- 4: Given the above values of $\underline{\alpha}_i$, $\overline{\alpha}_i$, and $\alpha_{c,i}$, find, using the ordinary least squares (OLS) method, the row vectors $\underline{\tilde{a}}_i$, $\overline{\tilde{a}}_i$, and $\tilde{a}_{c,i}$, respectively, that guide the evolution of the states in the p-augmented LTI approximation $\tilde{x}_i[k+1] = \tilde{a}_i\tilde{x}_i[k] + \tilde{b}_i^w w_i[k]$.
- 5: Propagate the dynamics according to the obtained OLS estimates and calculate the mean squared error (MSE) between the propagated states and the observed state trajectory.
- 6: **if** MSE is lesser for the α_i case **then**
- 7: Set $\overline{\alpha_i} = \alpha_{c,i}$.
- 8: **else if** MSE is lesser for the $\overline{\alpha_i}$ case then
- 9: Set $\alpha_i = \alpha_{c,i}$.
- 10: **end if**
- 11: Terminate if $|\overline{\alpha_i} \alpha_i| < \varepsilon$, else return to step 3.
- 12: end for

by observing the state trajectory of (34), i.e., $\{x[0], x[1], \ldots, x[K+1]\}$, and the process noise w[k] being independent and identically distributed (i.i.d.) zero-mean Gaussian.

Thus, prior to characterizing the sample complexity of the OLS method for the p-augmented LTI approximation of the DT-FODS, we define a few quantities of interest. The *finite-time controllability Gramian* of the approximated system (34), W_t , is defined by

$$W_t := \sum_{j=0}^{t-1} \tilde{A}^j (\tilde{A}^j)^\mathsf{T}. \tag{39}$$

Intuitively, the controllability Gramian gives a quantitative measure of how much the system is excited when induced by the process noise w[k] acting as an input to the system.

Additionally, given a symmetric matrix $A \in \mathbb{R}^{d \times d}$, we define $\lambda_{\max}(A)$ and $\lambda_{\min}(A)$ to denote, respectively, the maximum and minimum eigenvalues of the matrix A.

Lastly, for any square matrix $A \in \mathbb{R}^{d \times d}$, the spectral radius of the matrix A, $\rho(A)$, is given by the largest absolute value of its eigenvalues. Also, the

operator norm of a matrix is denoted by

$$||A||_{\text{op}} = \inf\{c \ge 0 : ||Av|| \le c||v|| \text{ for all } v \in V\}.$$

Hence, we have the following result that characterizes the sample complexity of the above OLS method for the DT-FODS approximation. Fix $\delta \in (0,1/2)$ and consider the *p*-augmented system in (34), where $\tilde{A} \in \mathbb{R}^{d \times d}$ is a marginally stable matrix (i.e., $\rho(\tilde{A}) \leq 1$) and $w[k] \sim \mathcal{N}(0, \sigma^2 I)$. Then, there exist universal constants c, C > 0 such that,

$$\mathbb{P}\left[\left\|\underline{\tilde{A}}[K] - \tilde{A}\right\|_{\text{op}} \le \frac{C}{\sqrt{K\lambda_{\min}(W_k)}} \times \sqrt{d\log\left(\frac{d}{\delta}\right) + \log\det\left(W_K W_k^{-1}\right)}\right] \\ \ge 1 - \delta, \tag{40}$$

for any k, such that

$$\frac{K}{k} \ge c \left(d \log \left(\frac{d}{\delta} \right) + \log \det \left(W_K W_k^{-1} \right) \right) \tag{41}$$

holds.

Remark 1. We note here that although the operator norm parameter estimation error in (40) is stated in terms of \tilde{A} , the operator norm errors, associated with the matrices $A_0, A_1, \ldots, A_{p-1}$, are strictly lesser compared to $\left\| \tilde{\underline{A}}[K] - \tilde{A} \right\|_{\text{op}}$, since $A_0, A_1, \ldots, A_{p-1}$ are submatrices of \tilde{A} , and for any operator norm, the operator norm of a submatrix is upper bounded by one of the whole matrix (see Lemma A.9 of (Foucart and Rauhut, 2013) for a proof).

Additionally, it is worth mentioning that a similar finite-sample complexity bound similar to the one presented before can also be derived when we consider the ordinary least squares identification of the spatial parameters of a DT-FODS with inputs. For instance, within the purview of epileptic seizure mitigation using intracranial EEG data, the objective of the former is to suppress the overall length or duration of an epileptic seizure. Thus, the goal is steering the state of the neurophysiological system in consideration away from seizure-like activity, using a control strategy like model predictive control (Chatterjee et al., 2020).

9. Minimum-energy state estimation

Most of the estimators that exist for fractional-order dynamical systems are obtained under the assumption that the disturbance and noise has Gaussian distribution (Sabatier et al., 2012; Sierociuk and Dzieliński, 2006; Safarinejadian et al., 2018, 2016; Miljković et al., 2017; Najar et al., 2009). Meanwhile, such assumption is not realistic in the context of neural systems as disturbance frequencies can only lie within a specific frequency band. Therefore, in what follows, we present the so-called *minimum-energy state estimation*, where it is assumed that the disturbance and noise are unknown, but deterministic and bounded uncertainties.

Now, consider a left-bounded sequence $\{x[k]\}_{k\in\mathbb{Z}}$ over k, i.e., with $\limsup_{k\to-\infty} ||x[k]|| < \infty$. Then, the Grünwald-Letnikov fractional-order difference, for any $\alpha \in \mathbb{R}^+$, can be re-written as

$$\Delta^{\alpha} x[k] := \sum_{j=0}^{\infty} c_j^{\alpha} x[k-j], \quad c_j^{\alpha} = (-1)^j {\alpha \choose j},$$

$${\alpha \choose j} = \begin{cases} 1 & \text{if } j = 0, \\ \prod_{j=0}^{j-1} \frac{\alpha - i}{i+1} = \frac{\Gamma(\alpha + 1)}{\Gamma(j+1)\Gamma(\alpha - j + 1)} & \text{if } j > 0, \end{cases}$$

$$(42)$$

for all $j \in \mathbb{N}$. The summation in (42) is well-defined from the uniform boundedness of the sequence $\{x[k]\}_{k \in \mathbb{Z}}$ and the fact that $|c_j^{\alpha}| \leq \frac{\alpha^j}{j!}$, which implies that the sequence $\{c_j^{\alpha}\}_{j \in \mathbb{N}}$ is absolutely summable for any $\alpha \in \mathbb{R}^+$ (Alessandretti et al., 2020; Sopasakis and Sarimveis, 2017).

With the above ingredients, a discrete-time fractional-order dynamical network with additive disturbance can be described, respectively, by the state evolution and output equations

$$\sum_{i=1}^{l} A_i \Delta^{a_i} x[k+1] = \sum_{i=1}^{r} B_i \Delta^{b_i} u[k] + \sum_{i=1}^{s} G_i \Delta^{g_i} w[k], \tag{43a}$$

$$z[k] = C'_k x[k] + v'[k],$$
 (43b)

with the variables $x[k] \in \mathbb{R}^n$, $u[k] \in \mathbb{R}^m$, and $w[k] \in \mathbb{R}^p$ denoting the state, input, and disturbance vectors at time step $k \in \mathbb{N}$, respectively. The scalars $a_i \in \mathbb{R}^+$ with $1 \le i \le l$, $b_i \in \mathbb{R}^+$ with $1 \le i \le r$, and $g_i \in \mathbb{R}^+$ with

 $1 \leq i \leq s$ are the fractional-order coefficients corresponding, respectively, to the state, the input, and the disturbance. The vectors $z[k], v'[k] \in \mathbb{R}^q$ denote, respectively, the output and measurement disturbance at time step $k \in \mathbb{N}$. We assume that the (unknown but deterministic) disturbance vectors are bounded as

$$||w[k]|| \le b_w, ||v'[k]|| \le b_{v'}, k \in \mathbb{N},$$
 (44)

for some scalars $b_w, b_{v'} \in \mathbb{R}^+$. We also assume that the control input u[k] is known for all time steps $k \in \mathbb{N}$. We denote by x[0] = x(0) the initial condition of the state at time k = 0. In the computation of the fractional-order difference, we assume that the system is *causal*, i.e., the state, input, and disturbances are all considered to be zero before the initial time (i.e., x[k] = 0, u[k] = 0, and w[k] = 0 for all k < 0).

Next, consider the quadratic weighted least-squares objective function

$$\mathcal{J}\left(x[0], \{w[i]\}_{i=0}^{N-1}, \{v'[j]\}_{j=1}^{N}\right) = \sum_{i=0}^{N-1} w[i]^{\mathsf{T}} Q_i^{-1} w[i] + \sum_{j=1}^{N} v'[j]^{\mathsf{T}} R_j^{-1} v'[j] + (x[0] - \hat{x}_0)^{\mathsf{T}} P_0^{-1} (x[0] - \hat{x}_0),$$
(45)

subject to the constraints

$$\sum_{i=1}^{l} A_i \Delta^{a_i} x[k+1] = \sum_{i=1}^{r} B_i \Delta^{b_i} u[k] + \sum_{i=1}^{s} G_i \Delta^{g_i} w[k]$$
 (46a)

and

$$z[k] = C'_k x[k] + v'[k],$$
 (46b)

for some $N \in \mathbb{N}$, with the weighting matrices Q_i ($0 \le i \le N-1$), R_j ($1 \le j \le N$), and P_0 chosen to be symmetric and positive definite, and \hat{x}_0 chosen to be the *a priori* estimate of the system's initial state. The minimum-energy estimation procedure seeks to solve the following optimization problem

$$\begin{array}{ll} & \underset{\{x[k]\}_{k=0}^{N}, \{w[i]\}_{i=0}^{N-1}, \{v'[j]\}_{j=1}^{N}}{minimize} & \mathcal{J}\left(x[0], \{w[i]\}_{i=0}^{N-1}, \{v'[j]\}_{j=1}^{N}\right) \\ & \text{subject to} & (46a) \text{ and } (46b), \end{array} \tag{47}$$

for some $N \in \mathbb{N}$.

To derive the solution to (47), we first start with some alternative formulations of the discrete-time fractional-order dynamical network (DT-FODN)

in (43a) and (43b) and relevant definitions that will be used in the sequel. Then, we present the solution and some additional properties of the derived solution, i.e., the exponential input-to-state stability of the estimation error.

In what follows, we consider the mild technical assumption that $\sum_{i=1}^{l} A_i$

is invertible. Additionally, we consider a truncation of the last \mathfrak{v} temporal components of (43a), which we will refer to as the \mathfrak{v} -approximation for the DT-FODN. That being said, the DT-FODN model in (43a) can be equivalently written as

$$x[k+1] = \sum_{j=1}^{\infty} \check{A}_j x[k-j+1] + \sum_{j=0}^{\infty} \check{B}_j u[k-j] + \sum_{j=0}^{\infty} \check{G}_j w[k-j], \quad (48)$$

where $\check{A}_j = -\hat{A}_0^{-1}\hat{A}_j$, $\check{B}_j = \hat{A}_0^{-1}\hat{B}_j$, and $\check{G}_j = \hat{A}_0^{-1}\hat{G}_j$ with $\hat{A}_j = \sum_{i=1}^l A_i c_j^{a_i}$, $\hat{B}_j = \sum_{i=1}^r B_i c_j^{b_i}$, and $\hat{G}_j = \sum_{i=1}^s G_i c_j^{g_i}$. Furthermore, for any positive integer $\mathfrak{v} \in \mathbb{N}^+$, the DT-FODN model in (43a) can be recast as

$$\tilde{x}[k+1] = \tilde{A}_{\mathfrak{v}}\tilde{x}[k] + \tilde{B}_{\mathfrak{v}}u[k] + \tilde{G}_{\mathfrak{v}}r[k], \qquad \tilde{x}[0] = \tilde{x}_0, \tag{49a}$$

$$y[k+1] = C_{k+1}\tilde{x}[k+1] + v[k+1], \tag{49b}$$

where

$$r[k] = \sum_{j=v+1}^{\infty} \check{A}_j x[k-j+1] + \sum_{j=v+1}^{\infty} \check{B}_j u[k-j] + \sum_{j=0}^{\infty} \check{G}_j w[k-j],$$
 (50)

with the augmented state vector $\tilde{x}[k] = [x[k]^{\mathsf{T}}, \dots, x[k-\mathfrak{v}+1]^{\mathsf{T}}, u[k-1]^{\mathsf{T}}, \dots, u[k-\mathfrak{v}]^{\mathsf{T}}]^{\mathsf{T}} \in \mathbb{R}^{\mathfrak{v} \times (n+m)}$ and appropriate matrices $\tilde{A}_{\mathfrak{v}}, \tilde{B}_{\mathfrak{v}}$, and $\tilde{G}_{\mathfrak{v}}$, where $\tilde{x}_0 = [x_0^{\mathsf{T}}, 0, \dots, 0]^{\mathsf{T}}$ denotes the initial condition. The matrices $\tilde{A}_{\mathfrak{v}}$ and $\tilde{B}_{\mathfrak{v}}$ are formed using the terms $\{\check{A}_j\}_{1 \leq j \leq \mathfrak{v}}$ and $\{\check{B}_j\}_{1 \leq j \leq \mathfrak{v}}$, while the remaining terms $\{\check{G}_j\}_{1 \leq j < \infty}$ and the state and input components not included in $\tilde{x}[k]$ are absorbed into the term $\tilde{G}_{\mathfrak{v}}r[k]$. Furthermore, we refer to (49a) as the \mathfrak{v} -approximation of the DT-FODN presented in (43a).

To obtain the minimum-energy estimator, let us consider the quadratic weighted least-squares objective function

$$\mathcal{J}\left(\tilde{x}[0], \{r[i]\}_{i=0}^{N-1}, \{v[j]\}_{j=1}^{N}\right) = \sum_{i=0}^{N-1} r[i]^{\mathsf{T}} Q_i^{-1} r[i] + \sum_{j=1}^{N} v[j]^{\mathsf{T}} R_j^{-1} v[j] + (\tilde{x}[0] - \hat{x}_0)^{\mathsf{T}} P_0^{-1} (\tilde{x}[0] - \hat{x}_0),$$
 (51)

subject to the constraints

$$\bar{x}[k+1] = \tilde{A}_{\mathfrak{v}}\bar{x}[k] + \tilde{B}_{\mathfrak{v}}u[k] + \tilde{G}_{\mathfrak{v}}\bar{r}[k], \tag{52a}$$

$$y[k+1] = C_{k+1}\bar{x}[k+1] + \bar{v}[k+1], \tag{52b}$$

for some $N \in \mathbb{N}$. The weighting matrices Q_i ($0 \le i \le N-1$) and R_j ($1 \le j \le N$) are chosen to be symmetric and positive definite. The term \hat{x}_0 denotes the *a priori* estimate of the (unknown) initial state of the system, with the matrix P_0 being symmetric and positive definite.

Subsequently, we consider the weighted least-squares optimization problem

$$\begin{array}{ll} & \underset{\{\bar{x}[k]\}_{k=0}^{N}, \{\bar{r}[i]\}_{i=0}^{N-1}, \{\bar{v}[j]\}_{j=1}^{N}}{minimize} & \mathcal{J}\left(\tilde{x}[0], \{r[i]\}_{i=0}^{N-1}, \{v[j]\}_{j=1}^{N}\right) \\ & \text{subject to} & (52a) \text{ and } (52b), \end{array}$$
(53)

for some $N \in \mathbb{N}$. Denote by $\hat{x}[k]$ the state vector that corresponds to the solution of the optimization problem (53). Then, $\hat{x}[k]$ satisfies the recursion

$$\hat{x}[k+1] = \tilde{A}_{v}\hat{x}[k] + \tilde{B}_{v}u[k] + K_{k+1}\left(y[k+1] - C_{k+1}\left(\tilde{A}_{v}\hat{x}[k] + \tilde{B}_{v}u[k]\right)\right),$$
(54)

given $0 \le k \le N-1$, with initial conditions specified for \hat{x}_0 and $\{u[j]\}_{j=0}^k$, and with the update equations

$$K_{k+1} = M_{k+1}C_{k+1}^{\mathsf{T}}(C_{k+1}M_{k+1}C_{k+1}^{\mathsf{T}} + R_{k+1})^{-1}, \tag{55a}$$

$$M_{k+1} = \tilde{A}_{\mathfrak{v}} P_k \tilde{A}_{\mathfrak{v}}^{\mathsf{T}} + \tilde{G}_{\mathfrak{v}} Q_k \tilde{G}_{\mathfrak{v}}^{\mathsf{T}}, \tag{55b}$$

and

$$P_{k+1} = (I - K_{k+1}C_{k+1})M_{k+1}(I - K_{k+1}C_{k+1})^{\mathsf{T}} + K_{k+1}R_{k+1}K_{k+1}^{\mathsf{T}}$$

= $(I - K_{k+1}C_{k+1})M_{k+1}$, (55c)

with symmetric and positive definite P_0 .

Notice that the dynamics of the recursion in (54) (with the initial conditions on \hat{x}_0 and the values of $\{u[j]\}_{j=0}^k$ being known) along with the update equations (55) together solve (53). It is interesting to note here that the output term y[k+1] presented in (52b) and (54) is the output of the \mathfrak{v} -approximated system (49), which, in turn, is simply a subset of the outputs z[k+1] obtained from (43b), truncated \mathfrak{v} time steps in the past, provided

v[k] and C_k are formed from the appropriate blocks of v'[k] and C'_k for all $k \in \mathbb{N}$.

Secondly, the minimum-energy estimator has exponential input-to-state stability of the estimation error.

In order to prove the exponential input-to-state stability of the minimumenergy estimation error, we need to consider the following mild technical assumptions. Specifically, there exist constants $\underline{\alpha}, \overline{\alpha}, \beta, \gamma \in \mathbb{R}^+$ such that

$$\underline{\alpha}I \preceq \tilde{A}_{\mathfrak{v}}\tilde{A}_{\mathfrak{v}}^{\mathsf{T}} \preceq \overline{\alpha}I, \quad \tilde{G}_{\mathfrak{v}}\tilde{G}_{\mathfrak{v}}^{\mathsf{T}} \preceq \beta I, \text{ and } C_k^{\mathsf{T}}C_k \preceq \gamma I,$$
 (56)

for all $k \in \mathbb{N}$.

Additionally, notice that the *state transition matrix* for the dynamics in (49a) is given by

$$\Phi(k, k_0) = \tilde{A}_{\mathfrak{p}}^{(k-k_0)}, \quad \text{with} \quad \Phi(k_0, k_0) = I,$$
(57)

for all $k \geq k_0 \geq 0$. We also consider the discrete-time controllability Gramian associated with the dynamics (49a) described by

$$W_c(k, k_0) = \sum_{i=k_0}^{k-1} \Phi(k, i+1) \tilde{G}_{\mathfrak{v}} \tilde{G}_{\mathfrak{v}}^{\mathsf{T}} \Phi^{\mathsf{T}}(k, i+1), \tag{58}$$

and the discrete-time observability Gramian associated with (49a) to be

$$W_o(k, k_0) = \sum_{i=k_0+1}^k \Phi^{\mathsf{T}}(i, k_0) C_i^{\mathsf{T}} C_i \Phi(i, k_0), \tag{59}$$

for $k \geq k_0 \geq 0$. We also make the following assumptions regarding complete uniform controllability and complete uniform observability of the \mathfrak{v} -approximated system in (49a).

As such, we have to also consider that the \mathfrak{v} -approximated system (49a) is completely uniformly controllable, i.e., there exist constants $\delta \in \mathbb{R}^+$ and $N_c \in \mathbb{N}^+$ such that

$$W_c(k+N_c,k) \succeq \delta I,$$
 (60)

for all $k \geq 0$. And, similarly, the \mathfrak{v} -approximated system (49a) is completely uniformly observable, i.e., there exist constants $\varepsilon \in \mathbb{R}^+$ and $N_o \in \mathbb{N}^+$ such that

$$W_o(k + N_o, k) \succeq \varepsilon \Phi^{\mathsf{T}}(k + N_o, k) \Phi(k + N_o, k), \tag{61}$$

for all $k \geq 0$.

Next, we also present an assumption certifying lower and upper bounds on the weight matrices Q_k and R_{k+1} in (51). That is, without loss of generality, we assume that the weight matrices Q_k and R_{k+1} satisfy

$$\underline{\vartheta}I \preceq Q_k \preceq \overline{\vartheta}I \quad \text{and} \quad \underline{\rho}I \preceq R_{k+1} \preceq \overline{\rho}I,$$
 (62)

for all $k \geq 0$ and constants $\underline{\vartheta}, \overline{\vartheta}, \rho, \overline{\rho} \in \mathbb{R}^+$.

Hence, it is possible to we establish lower and upper bounds for the matrix P_k required to show that the estimation error is exponentially input-to-state stable. Specifically, the minimum-energy estimation error e[k], given by

$$e[k] = \hat{x}[k] - \tilde{x}[k], \tag{63}$$

is such that there exist constants $\sigma, \tau, \chi, \psi \in \mathbb{R}^+$ with $\tau < 1$ such that the estimation error e[k] satisfies

$$||e[k]|| \le \max \left\{ \sigma \tau^{k-k_0} ||e[k_0]||, \ \chi \max_{k_0 \le i \le k-1} ||r[i]||, \ \psi \max_{k_0 \le j \le k-1} ||v[j+1]|| \right\}$$
 (64)

for all $k \ge k_0 \ge \max\{N_c, N_o\}$.

It is interesting to note that the bound on the estimation error e[k] in (64) actually depends on ||r[i]||, where $k_0 \leq i \leq k-1$ for all $i \in \mathbb{N}$. In fact, a distinguishing feature of DT-FODN is the presence of a finite non-zero disturbance term in the input-to-state stability bound of the tracking error when tracking a state other than the origin. This disturbance is dependent on the upper bounds on the non-zero reference state being tracked as well as the input. While the linearity of the Grünwald-Letnikov fractional-order difference operator allows one to mitigate this issue in the case of tracking a non-zero exogenous state by a suitable change of state and input coordinates, this approach is not one we can pursue in this paper, since the state we wish to estimate is unknown. However, it can be shown that as the value of \mathfrak{v} in the \mathfrak{v} -approximation increases, the upper bound associated with ||r[i]|| decreases drastically since the \mathfrak{v} -approximation gives us progressively better representations of the unapproximated system. This further implies that ||r|i|| in (64) stays bounded, with progressively smaller upper bounds associated with ||r[i]|| (and hence, ||e[k]||) with increasing \mathfrak{v} .

Lastly, the estimation error associated with the minimum-energy estimation process in (63) is defined in terms of the state of the v-approximated system $\tilde{x}[k]$. In reality, as detailed above, with larger values of \mathfrak{v} , the \mathfrak{v} -approximated system approaches the real network dynamics, and thus we obtain an expression for the estimation error with respect to the real system in the limiting case, where the input-to-state stability bound as presented in (64) holds.

10. Fractional optimal control

Fractional optimal control finds the optimal control strategy to manipulate a fractional-order dynamical system to achieve a specific goal. Usually the goal is to achieve a certain desired state behavior while minimizing the amount of control effort (Riewe, 1996). The fractional optimal control problem with a finite-time horizon can be formulated as follows:

(cost function) minimize
$$\int_{t_0}^{T} (\mathbf{x}(t) - \mathbf{x}_d(t))^{\mathsf{T}} Q(\mathbf{x}(t) - \mathbf{x}_d(t)) + \mathbf{u}(t)^{\mathsf{T}} R \mathbf{u}(t) dt$$
(constraints) subject to
$$\Delta^{\alpha} \mathbf{x}(t) = A \mathbf{x}(t) + B \mathbf{u}(t)$$
other linear constraints on $\mathbf{x}(t)$ and $\mathbf{u}(t)$,
(65)

where $\mathbf{x}(t) \in \mathbb{R}^n$ is the state of the system, $\mathbf{x}_d(t) \in \mathbb{R}^n$ is the desired state of the system, $\mathbf{u}(t) \in \mathbb{R}^m$ is the control input, Q is the cost on the state achieving the desired behavior, R is the cost on the control effort, Δ^{α} is the Caputo fractional-order derivative, $A \in \mathbb{R}^{n \times n}$ is the state matrix, and $B \in \mathbb{R}^{n \times m}$ is the control input matrix.

Many mathematical techniques for solving fractional optimal control problems have been proposed, including numerical solvers (Nemati et al., 2019; Baleanu et al., 2009; Agrawal and Baleanu, 2007; Agrawal, 2004) and discrete methods (Almeida and Torres, 2015). Other works have considered fractional optimal control using the following schemes, including distributed fractional optimal control (Zaky and Machado, 2017), finite-time horizon (Biswas and Sen, 2011), multi-dimensional (Agrawal et al., 2010), Euler-Lagrange formulation (Frederico and Torres, 2008, 2007; Torres and Malinowska, 2012; Agrawal, 2002), and reinforcement learning (Gupta et al., 2021). Furthermore, fractional optimal control has been used in the following applications cloud computing (Ghorbani et al., 2014), regulating diabetes (Ghorbani and Bogdan, 2014, 2013), cyber-physical systems (Bogdan and Marculescu, 2011), regulating heart disease (Bogdan et al., 2012a,

2013a), data-centers-on-chip (Bogdan, 2015), and power management (Bogdan et al., 2012b, 2013b), and chemical processing plants (Petráš, 2021).

Fractional optimal control is at the core of receding horizon approaches referred to as model predictive control, and overviewed in more detail next.

11. Model predictive control

Model predictive control (MPC) is a control strategy that allows the control of processes while satisfying a set of constraints. At its core, MPC uses explicit process models (which may be linear or nonlinear) to predict how a plant will respond to arbitrary inputs. For each instant of time, an MPC algorithm seeks to optimize plant behavior in the future by computing a series of control inputs over a time horizon called the *prediction horizon* by solving an optimization problem – often with constraints. Once this step is complete, the computed control inputs corresponding to the first subsection of the prediction horizon (called the *control horizon*) are then sent to the plant. This procedure is then repeated at subsequent control intervals (Qin and Badgwell, 2003). This receding horizon strategy implicitly introduces *closed-loop feedback*.

Next, we consider the case where the predictive model is a linear fractional-order system. Based on the state signal's evolution predicted by the model, and by regarding the impact of an arbitrary control input signal in the state's evolution, we can set out to adapt the stimulation signal in real-time by choosing the parameters that lead to stimulation signals within a safe range towards optimizing some measure of performance that encapsulates the goal of steering abnormal activity to normal ranges. In general, however, our predictive model will not precisely match the real dynamics of the system. Therefore, our proposed stimulation strategy will periodically re-evaluate the current estimated state and corresponding predictions and re-compute the appropriate optimal stimulation strategy.

First, in the fractional-order model predictive control framework, we will focus on the design of a model predictive controller for a (possibly time-varying) discrete-time fractional-order dynamical system model

$$\Delta^{\alpha} x[k+1] = A_k x[k] + B_k u[k] + B_k^w w[k], \tag{66}$$

where w[k] denotes a sequence of independent and identically distributed random vectors, following an $\mathcal{N}(0,\Sigma)$ distribution (with the covariance matrix $\Sigma \in \mathbb{R}^{n \times n}$) and B_k^w denotes the matrix of weights that scales the noise

term w[k]. The objective is to design the feedback controller such that it minimizes a quadratic cost functional of the input and state vectors over a finite time horizon P (the prediction horizon). In other words, the objective is to determine the sequence of control inputs $u[k], \ldots, u[k+P-1]$ that minimizes a quadratic cost function of the form

where $Q_{k+1}, \ldots, Q_{k+P} \in \mathbb{R}^{n \times n}$ and $R_k, \ldots, R_{k+P-1} \in \mathbb{R}^{n_u \times n_u}$ are given positive semidefinite matrices. Here, $Q \in \mathbb{R}^{n \times n}$ is a positive semidefinite matrix if $x^\mathsf{T} Q x \geq 0$, for every $x \in \mathbb{R}^n$, and $\|x\|_Q = \sqrt{x^\mathsf{T} Q x}$ in that case.

The quadratic term on the input, which represents the electrical neurostimulation signal, is intended to add a penalization term for stimulating the patient too harshly, since this may be unsafe, create discomfort for the patient, or result in harmful psychological effects (Moratti and Patterson, 2014). It is also interesting to note that even if we need the estimation of the system states in the above problem, the presence of a separation principle for discrete-time fractional-order systems (Chatterjee et al., 2019) gives us guarantees that we can perform model predictive control with state estimation for these systems.

Note that, here, P is called the *prediction horizon*, and the framework only deploys the control strategy associated with the first M time steps (referred to as the *control horizon*). Simply speaking, after we reach state x[k+M-1], we update k with k+M-1 and recompute the new solution. This way, we have robust solutions, since, by design, the optimal strategy is constantly being re-evaluated based on the short-term control action implementation of a long-term prediction (Bequette, 2013; Petráš, 2021).

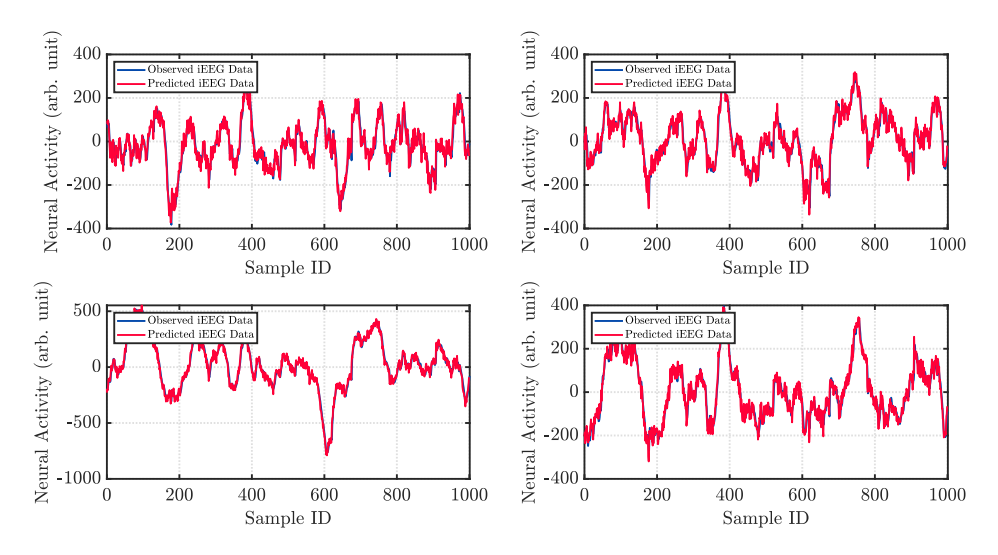


Figure 2: Performance of our system identification approach on real-life intracranial EEG data.

12. Applications in cyber-neural systems

12.1. System identification

We present some preliminary results regarding the performance of the above approach. Specifically, we use 1000 noisy measurements taken from 4 channels of an intracranial electroencephalographic (iEEG) signal which records the brain activity of subjects undergoing epileptic seizures. The signals were recorded and digitized at a sampling rate of 512 Hz at the Hospital of the University of Pennsylvania, Philadelphia, PA. Subdural grid and strip electrodes were placed at specialized locations (dictated by a multidisciplinary team of neurologists, neurosurgeons, and a radiologist), with the electrodes themselves consisting of linear and two-dimensional arrays spanning 2.3 mm in diameter and having a inter-contact spacing of 10 mm (Khambhati et al., 2015; Ashourvan et al., 2020).

The least squares optimization problems described in Section 8 are solved using CVX (Grant and Boyd, 2008, 2014) with the aid of a window-based approach using a finite subset of the entire range of measurements. This is done because the time series under consideration is nonlinear, and it is not possible to characterize the entire gamut of measurements using very few parameters. Figure 2 shows the performance of our method on the above data. Additionally, we also show in Figure 3 the variation of the error of the least

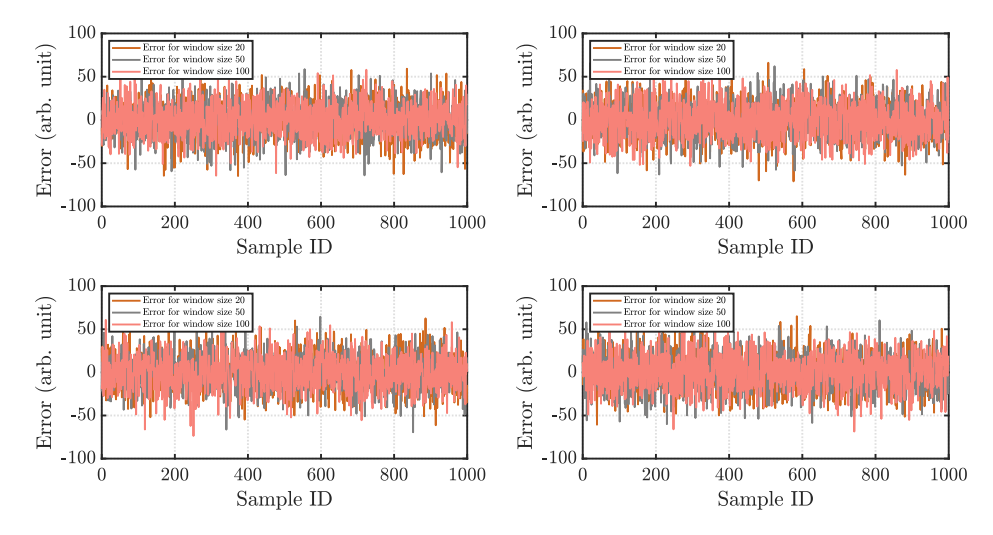


Figure 3: Variation of the error of the least squares prediction with respect to the observed data, with varying window sizes in the least squares optimization problems.

squares predictions with respect to the observed data, with varying window sizes in the least squares optimization problems. We see that the identified system parameters are able to predict the system states fairly closely, thus demonstrating that our approach can be used to learn the system parameters of a discrete-time fractional-order system.

12.2. Minimum-energy state estimation

In this section, we consider the performance of the minimum-energy estimation paradigm on real-world neurophysiological networks considering EEG data. Specifically, we use 150 noisy measurements taken from 4 channels of a 64-channel EEG signal which records the brain activity of subjects, as shown in Figure 4. The subjects were asked to perform a variety of motor and imagery tasks. Furthermore, the specific choice of the 4 channels was dictated due to them being positioned over the motor cortex of the brain, and, therefore, enabling us to predict motor actions such as the movement of the hands and feet. The data was collected using the BCI2000 system with a sampling rate of 160 Hz (Schalk et al., 2004; Goldberger et al., 2000). The spatial and temporal parameter components of the fractional-order system assumed to model the original EEG data were identified using the methods described in (Gupta et al., 2018a). The matrices $B_i = \begin{bmatrix} 1 & 1 & 1 \end{bmatrix}^T$ for all i.

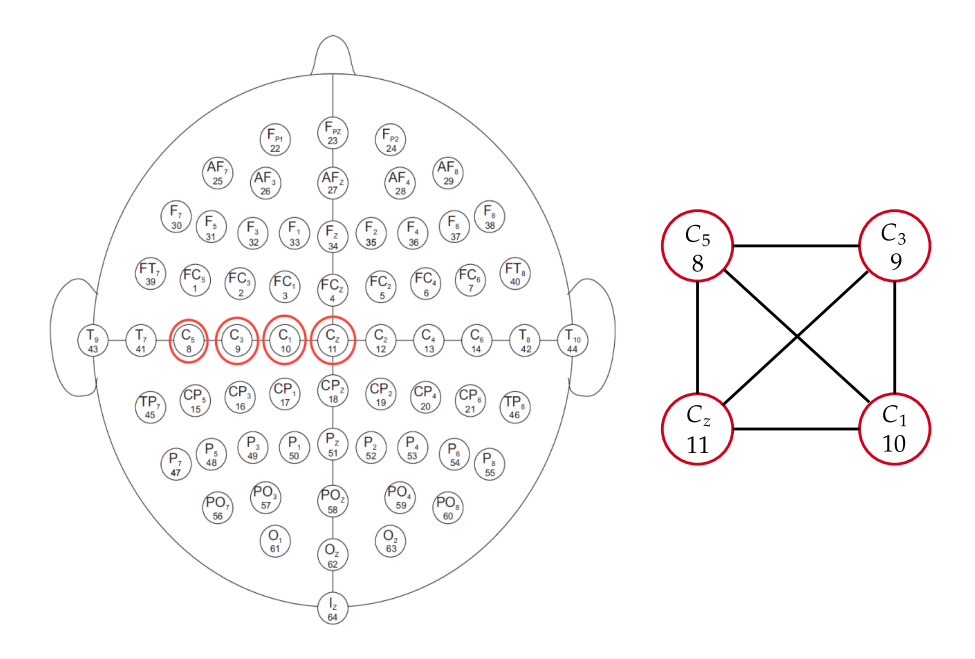


Figure 4: The distribution of the sensors for the measurement of EEG data is shown on the left. The channel labels are shown along with their corresponding numbers and the selected channels over the motor cortex are shown in red. The corresponding network formed by the EEG sensors is shown on the right.

The results of our approach, considering different values of \mathfrak{v} , are shown in Figures 5 and 6 (for $\mathfrak{v}=2$), Figures 7 and 8 (for $\mathfrak{v}=10$), and Figures 9 and 10 (for $\mathfrak{v}=20$), which show, respectively (for each value of \mathfrak{v}), the comparison between the measured output of the network with noise and the estimated response obtained from the minimum-energy estimator, and also the juxtaposition of the measurement error and the estimation error of the minimum-energy estimation process. We find that the minimum-energy estimator is successfully able to estimate the states in the presence of noise in both the dynamics and the measurement processes.

We also note from the Figures 5 and 6 that when $\mathfrak{v}=2$, we get comparatively larger estimation errors associated with the last 50 or so samples of Channel 4 and that this behavior can be mitigated by increasing the value of \mathfrak{v} , e.g., by choosing $\mathfrak{v}=10$ or $\mathfrak{v}=20$. This is in line with the discussion at the end of Section 9, and choosing a larger value of \mathfrak{v} can always, in practice, provide us with better estimation performances, as seen from this example.

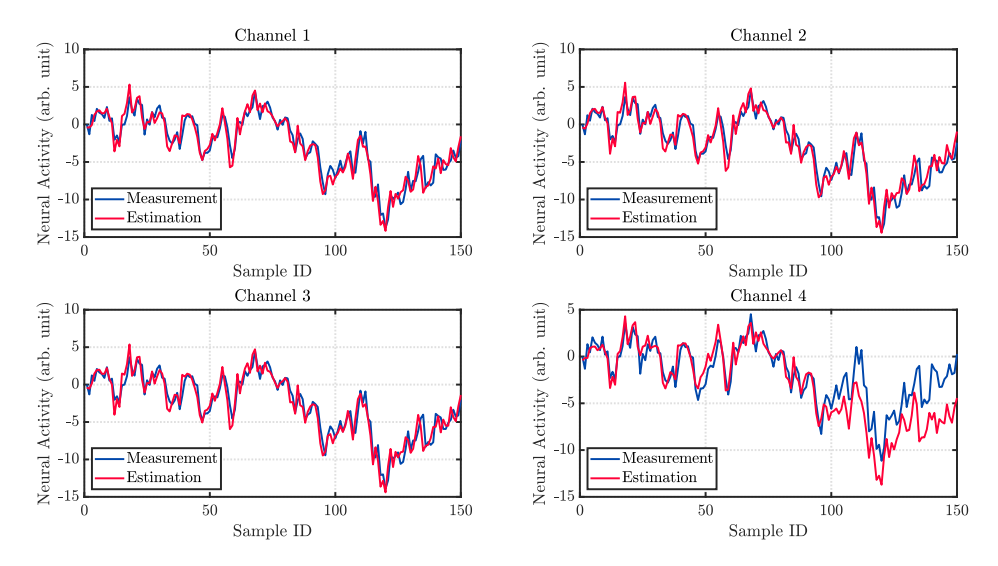


Figure 5: Comparison between the measured output of the \mathfrak{v} -augmented system (with $\mathfrak{v}=2$) versus the estimated output of a minimum-energy estimator implemented on the same, in the presence of process and measurement noises for 4 channels of a 64-channel EEG signal.

12.3. Neurostimulation using fractional-order model predictive control for epileptic seizure mitigation

In what follows, we propose to illustrate the use of the fractional-order system model predictive control (FOS-MPC) framework for neurostimulation in the context of mitigating epileptic seizures. We demonstrate the workings of the proposed approach on four different experimental scenarios relying primarily on intracranial electroencephalographic (iEEG) data: (i) an iEEG signal demonstrating an epileptic seizure simulated by the neural mass model proposed by Jansen and Rit (Jansen et al., 1993; Jansen and Rit, 1995); (ii) an iEEG signal simulated by a neural field model proposed by Martinet et al. in (Martinet et al., 2017) that replicates the spatiotemporal dynamics of a seizure; (iii) an iEEG signal simulated by the phenomenological 'Epileptor' model proposed in (Jirsa et al., 2014); and (iv) real-time iEEG signals for three human subjects undergoing epileptic seizures. For all of the above cases, we start by considering an epileptic seizure, captured by a linear fractional-order system (FOS) model, whose parameters are obtained through a system identification method using brainwave data obtained from iEEGs.

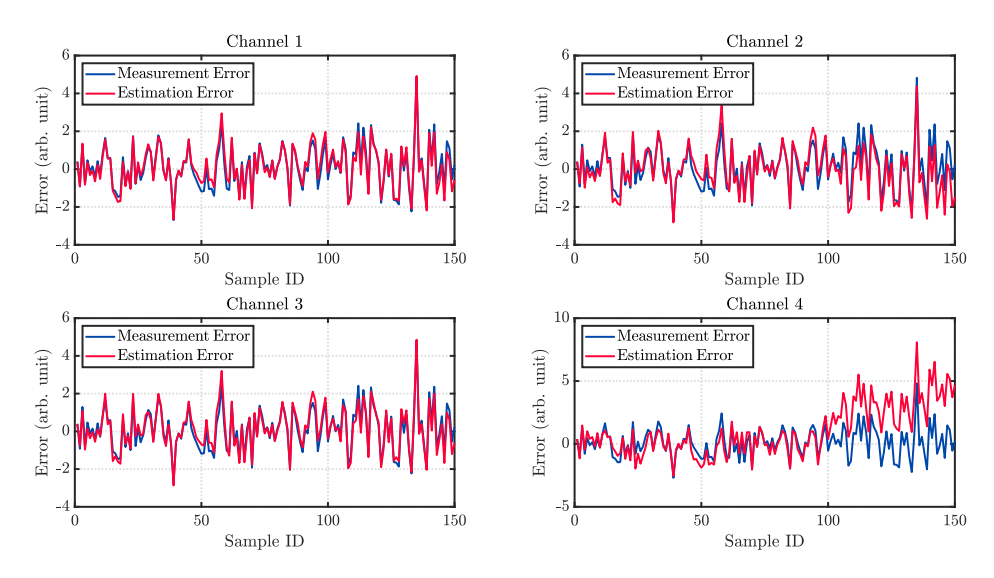


Figure 6: Comparison between the measurement error of the \mathfrak{v} -augmented system (with $\mathfrak{v}=2$) versus the estimation error of a minimum-energy estimator implemented on the same, in the presence of process and measurement noises for 4 channels of a 64-channel EEG signal.

12.3.1. Epileptic seizure simulated by the Jansen-Rit neural mass model

Although initially proposed to account for human EEG rhythms and visual evoked potentials, the Jansen-Rit neural mass model (Jansen and Rit, 1995) has also been used to shed light on human epileptiform brain dynamics (Wendling et al., 2000, 2016). The Jansen-Rit neural mass model is composed of three interacting subpopulations that include: the main subpopulation, the excitatory feedback subpopulation, and the inhibitory feedback subpopulation. The structure of the model is such that the main subpopulation comprises cells that receive neuronal signals in feedback from the excitatory and inhibitory subpopulations.

The use of neural mass models akin to the Jansen-Rit model in feedback control frameworks is well documented. All the works in (Wang et al., 2016; Xia et al., 2019; Wei et al., 2019c,a,b; Soltan et al., 2018) use neural mass models, in the control theory sense, for the suppression of epileptic seizures. In what follows, we will demonstrate the effectiveness of our proposed control strategy on a seizure simulated by the classical Jansen-Rit neural mass model with standard parameter values.

First, we need to determine the parameters A and α that model both spa-

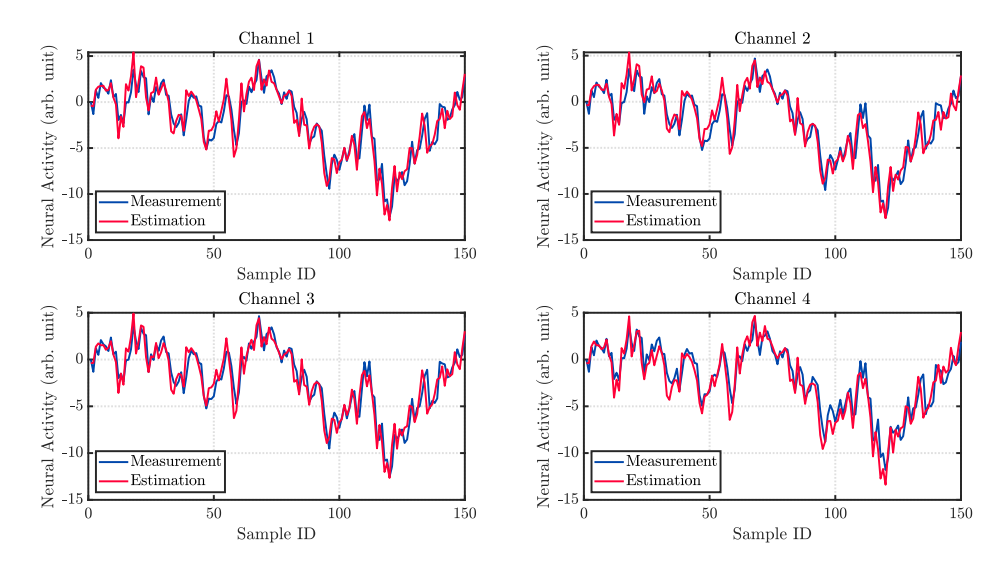


Figure 7: Comparison between the measured output of the \mathfrak{v} -augmented system (with $\mathfrak{v}=10$) versus the estimated output of a minimum-energy estimator implemented on the same, in the presence of process and measurement noises for 4 channels of a 64-channel EEG signal.

tial coupling and fractional coefficients, respectively, that craft the evolution of the state $x[k] \in \mathbb{R}^n$ in the fractional-order system (FOS) model.

$$\Delta^{\alpha} x[k+1] = Ax[k] + Bu[k] + B^{w}w[k], \tag{68}$$

with w[k] denoting additive white Gaussian noise (AWGN). Since the system is single-input-single-output (SISO), we have both A and α to be scalars. To identify the parameters A and α , we used the method proposed in (Gupta et al., 2018a). The parameters obtained are A = -0.0054 and $\alpha = 1.4881$. Furthermore, we assume that B = 1 and $B^w = 0.1$.

For the cost function in (67), we utilized $Q_k = I_n$, $R_k = I_{n_u}$, and $c_k = 0_{n_u \times 1}$ (with $n = n_u = 1$), to emphasize minimizing the overall energy in the measured iEEG signal, while penalizing slightly for overly aggressive stimulation. Furthermore, we included a safety linear constraint of $-5 \le u[k] \le 5$. Our predictive model was based on a (p = 15)-step (15 ms) predictive model approximation of the FOS plant, with a (P = 20)-step (20 ms) prediction horizon and (M = 10)-step (10 ms) control horizon. The results are presented in Figure 11, which provide evidence that the proposed stimulation strategy allows us to achieve amplitude suppression using a (time-

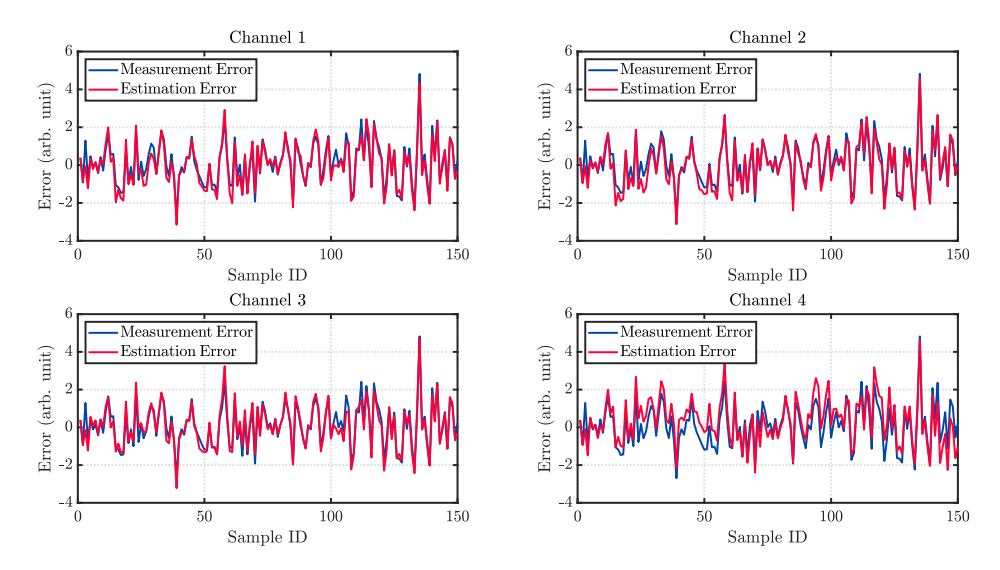


Figure 8: Comparison between the measurement error of the \mathfrak{v} -augmented system (with $\mathfrak{v}=10$) versus the estimation error of a minimum-energy estimator implemented on the same, in the presence of process and measurement noises for 4 channels of a 64-channel EEG signal.

varying) impulse-like stimulation scheme. Note that the actuation signal u_k kicks in at about the 4-second mark in the figure.

12.3.2. Epileptic seizure simulated by the mean-field model proposed by Martinet et al. (Martinet et al., 2017).

Next, we turn our attention towards a computational model that uses traveling wave dynamics to capture inter-scale coupling phenomena between large-scale neural populations in the cortex and small-scale groups in cortical columns (Martinet et al., 2017). Modeling the complex spatiotemporal dynamics of epileptic seizures is a challenging task, mainly because of the interaction of myriad scales in both time and space.

The neural field model proposed by Martinet et al. in (Martinet et al., 2017) is a modified version of the mean-field model proposed in (Steyn-Ross et al., 2013) that seeks to explain the phenomena, origin, and spatiotemporal dynamical properties of seizure propagation and spike-and-wave discharges (SWDs). Additionally, their work advances the hypothesis that increased diffusion of extracellular potassium concentrations in space influences the interlaced coupling of human seizures. In what follows, we will use the simulated seizure data obtained from the aforementioned model and then consider

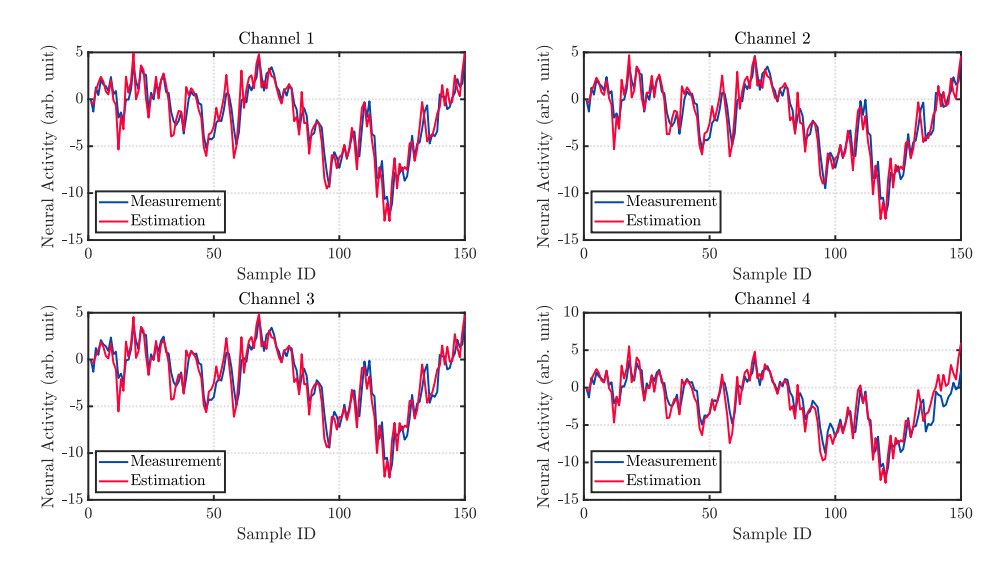


Figure 9: Comparison between the measured output of the \mathfrak{v} -augmented system (with $\mathfrak{v}=20$) versus the estimated output of a minimum-energy estimator implemented on the same, in the presence of process and measurement noises for 4 channels of a 64-channel EEG signal.

our closed-loop MPC neurostimulation scheme on the same model.

To determine the system parameters A and α in (68), we utilize roughly 2 seconds of pre-ictal activity captured by the model. Note that here, we will only consider n=4 channels for our proposed approach to mimic the capabilities available in the NeuroPace[®] RNS[®] device. Applying the methods in (Gupta et al., 2018a) yields the following FOS parameters:

$$A = \begin{bmatrix} 0.2969 & -0.0203 & -0.2922 & 0.0587 \\ 0.2574 & -0.1726 & -0.1905 & 0.1535 \\ 0.5348 & -0.1066 & -0.3471 & -0.0169 \\ 0.4007 & -0.6752 & 0.0044 & 0.3186 \end{bmatrix},$$
(69)

and

$$\alpha = \begin{bmatrix} 0.8114 & 0.8334 & 0.8034 & 0.8413 \end{bmatrix}^{\mathsf{T}}. \tag{70}$$

Additionally, we consider a single control signal u_k that affects all the channels equally, i.e., $B = \begin{bmatrix} 1 & 1 & 1 \end{bmatrix}^\mathsf{T}$ and the matrix of weights $B^w = 0.05I_4$, with I_4 being the 4×4 identity matrix.

Using the FOS-MPC neurostimulation strategy with $Q_k = I_n$, $R_k = I_{n_u}$, and $c_k = 0_{n_u \times 1}$ (with n = 4 and $n_u = 1$), and safety linear constraints of

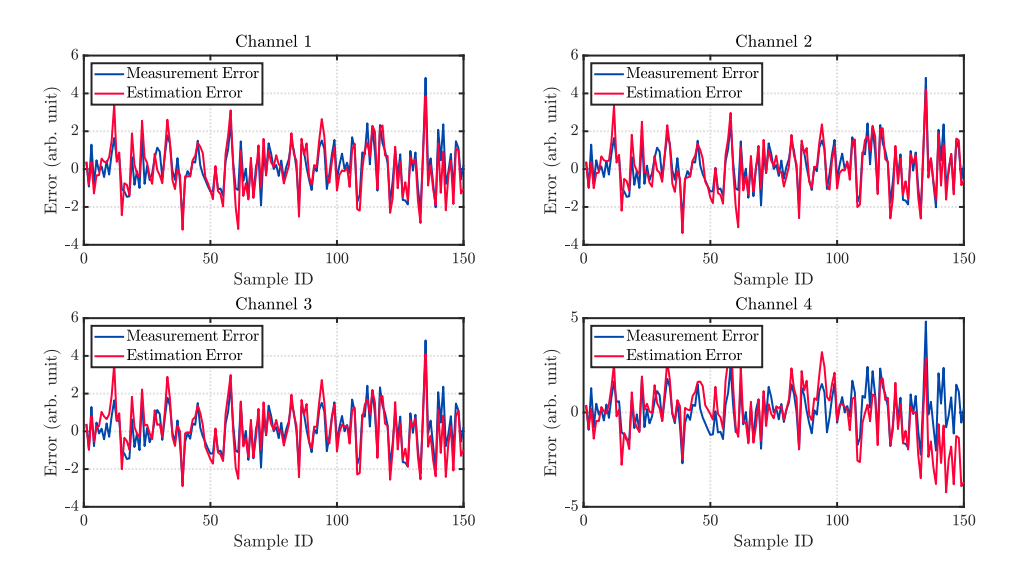


Figure 10: Comparison between the measurement error of the \mathfrak{v} -augmented system (with $\mathfrak{v}=20$) versus the estimation error of a minimum-energy estimator implemented on the same, in the presence of process and measurement noises for 4 channels of a 64-channel EEG signal.

 $-100 \le u[k] \le 100$, we find from Figure 12 that our proposed approach successfully suppresses seizure-like activity using a (time-varying) impulse-like stimulation scheme. In this case, we use a (p=10)-step (20 ms) predictive model approximation of the FOS plant, with a (P=10)-step (20 ms) prediction horizon, and (M=8)-step (16 ms) control horizon. Here too, the actuation signal u_k kicks in at about the 4-second mark.

12.3.3. Epileptic seizure simulated by the Epileptor, a phenomenological model of seizures by Jirsa et al. (Jirsa et al., 2014)

Next, we investigate the performance of our proposed approach on the Epileptor model (Jirsa et al., 2014), which is a phenomenological model able to accurately reproduce the dynamics of a wide variety of human epileptic seizures recorded with iEEG electrodes.

The Epileptor is a mathematical model proposed by Jirsa et al. in (Jirsa et al., 2014) and is based on analyzing experimental readings of iEEG seizure discharges in various human and animal subjects. At its core, the model consists of six coupled ordinary differential equations in three time scales. These equations are successfully able to model bistable dynamics between alternating fast discharges and inter-ictal activity, spike-and-wave events (SWEs),

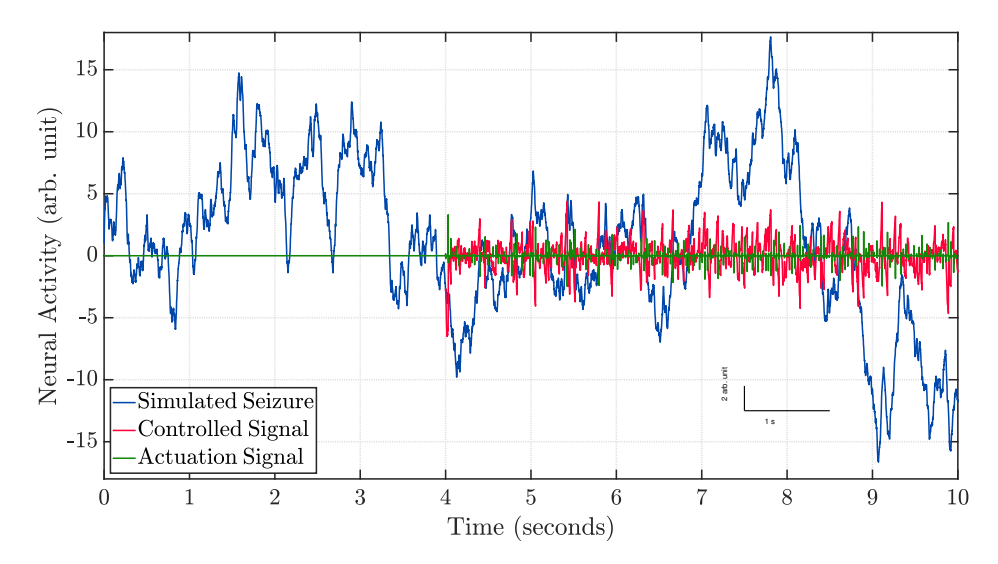


Figure 11: Results of the proposed FOS-MPC closed-loop neurostimulation strategy on an iEEG seizure simulated by the Jansen-Rit neural mass model. The simulated iEEG signal with the seizure is depicted in blue, the controlled signal is depicted in red, and the stimulation pulses are shown in green.

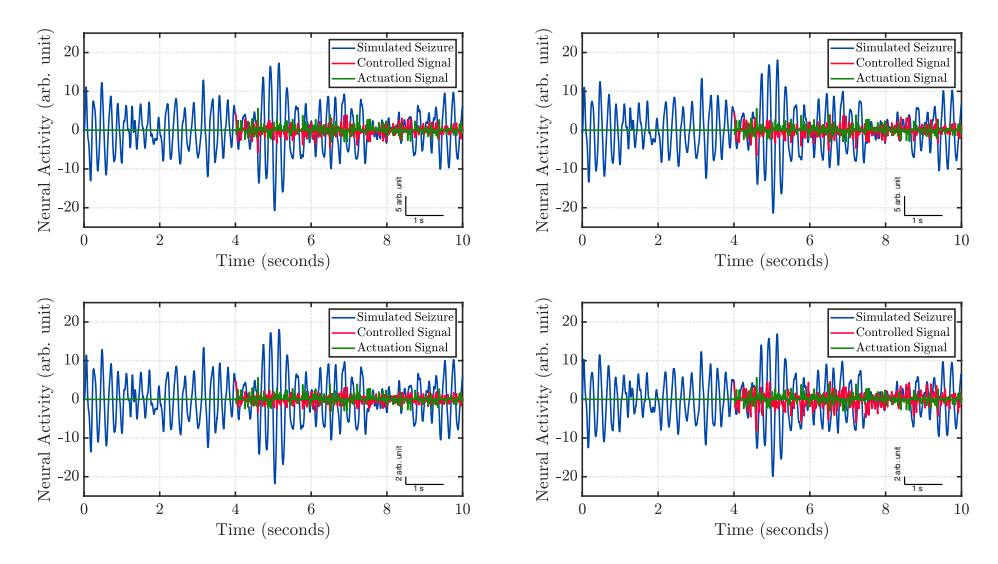


Figure 12: Results of the proposed FOS-MPC closed-loop neurostimulation strategy on an iEEG seizure simulated by the traveling wave dynamics model proposed in Martinet et al. (Martinet et al., 2017). The simulated iEEG signal with the seizure is depicted in blue, the controlled signal is depicted in red, and the stimulation pulses are shown in green.

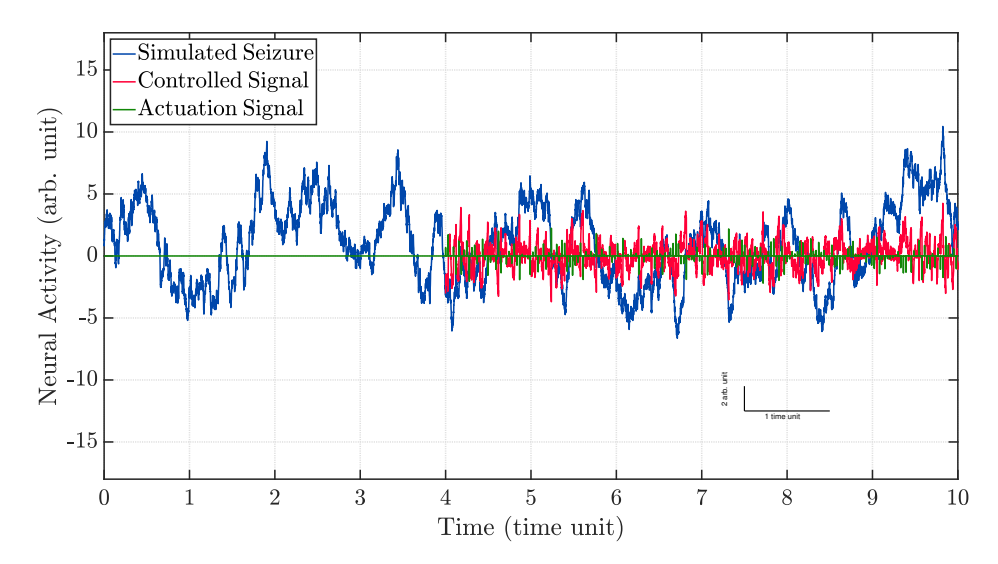


Figure 13: Results of the proposed FOS-MPC closed-loop neurostimulation strategy on an iEEG seizure simulated by the Epileptor model. The simulated iEEG signal with the seizure is depicted in blue, the controlled signal is depicted in red, and the stimulation pulses are shown in green.

and the evolution of the neural populations through the phenomena of seizure onset and offset. In what follows, we will use the simulated seizure data obtained from the Epileptor model and implement our closed-loop MPC neuromodulation scheme on it.

To determine the parameters A and α that model both spatial coupling and fractional coefficients, respectively, that craft the evolution of the state dynamics in (68), we use the method proposed in (Gupta et al., 2018a). Here, like the Jansen-Rit model, the system is SISO, and hence A and α are scalars. The parameters obtained are A = -0.0051 and $\alpha = 1.0614$. Furthermore, we assume that B = 1 and $B^w = 0.25$.

We implement the FOS-MPC neurostimulation strategy with $Q_k = I_n$, $R_k = I_{n_u}$, and $c_k = 0_{n_u \times 1}$ (with $n = n_u = 1$) and safety linear constraints of $-50 \le u[k] \le 50$. In this case, our predictive model was based on a (p = 20)-step predictive model approximation of the FOS plant, with a (P = 20)-step prediction horizon and (M = 10)-step control horizon. The results are presented in Figure 13, which provide evidence that the proposed stimulation strategy allows us to achieve amplitude suppression for a seizure simulated by the Epileptor model with standard parameter values.

13. Conclusions and directions for future research

Cyber-neural systems are becoming pervasive in today's society, yet they still lack the capability of performing real-time closed-loop control of neural activity. Control systems engineers will play a vital role in bringing this technology to reality as they develop the tools required by interdisciplinary teams involved in envisioning the next generation of neurotechnology.

That said, we provided a glance at some of the latest trends and techniques in fractional-order based system modeling, analysis, and closed-loop control towards the development of future neurotechnologies. In particular, we present results on system identification, state estimation, and closed-loop control in discrete-time fractional-order dynamical systems.

Notwithstanding, there is a plethora of interesting research directions which can be taken from here, aligned with each of the foundations pinpointed next.

13.1. System identification

System identification of fractional-order systems is an extremely under-explored field in general, with a lack of a systematic and unified theory, with some preliminary approaches utilizing wavelets (Flandrin, 1992), frequency-domain techniques (Adams et al., 2006; Dzieliński et al., 2011), or a sequential combination of wavelets and expectation-maximization (EM) (Gupta et al., 2018a).

Although approaches using the EM algorithm for linear (Gibson and Ninness, 2005) as well as nonlinear system identification (Schön et al., 2011) have existed in the literature for a while now, one immediately notices that there is a long-standing problem in characterizing theoretical robustness guarantees for the same. We can draw inspiration from preliminary analyses of finite-sample robustness guarantees for EM in (Wu et al., 2016; Balakrishnan et al., 2017; Yan et al., 2017) to characterize the sample complexity in identifying linear time-invariant (LTI) to do the same for the fractional-order systems.

In practice, it would be important to investigate approaches to identify the spatial and temporal parameters of fractional-order systems based on bootstrapping (Tjärnström, 1999), with alternating and progressively better identifications of the aforementioned parameters. Future work should focus on chalking out a general theory of identifying certain classes of fractional-order systems. Alternatively, one could also look into strategies behind using recurrent neural networks (RNNs) to identify the fractional-order systems' parameters. One of the most celebrated results in neural network theory, the *universal approximation theorem* (Hornik et al., 1989; Funahashi, 1989; Cybenko, 1989), states that continuous functions can be arbitrarily well-approximated by single-hidden-layer feedforward neural networks. While recent work (Hutter et al., 2021) seems to suggest the presence of allied results when RNNs are used to identify stable LTI systems optimally in the sense of metric entropy (Zames and Owen, 1993), it remains to be seen whether universal approximation theorem-like results can be derived when RNNs are used to identify fractional-order systems.

It would also be interesting to investigate fundamental information-theoretic connections between the number of samples needed to perform online system identification for fractional-order systems that would, in turn, allow for a more robust control design using the same. Furthermore, one could also potentially look into the number of samples needed to uniquely identify the parameters of fractional-order systems and whether different identified realizations potentially correspond to different fractional-order systems.

13.2. State estimation

Although fractional-order systems have found vast success in modeling the spatiotemporal properties of EEG, some of the properties accounted for by these models actually originate from unknown sources external to the system under consideration. Future work should focus on modeling these external sources by unknown input stimuli and then focus on state estimation of the resultant model with unknown inputs.

Real-time neural activity can be monitored to self-regulate brain function. This is known in the literature as neurofeedback (Marzbani et al., 2016), and it would be interesting to study how the introduction of feedback to such a system changes our perspectives on this problem.

Besides, whereas the construction of resilient state estimators grow over the last decade, little effort was put in developing resilient versions of state estimators for fractional-order systems. In particular, and given that suitable assumptions for the disturbance and noise do not rely on gaussianity assumptions, it would be imperative to build a resilient and attack-resistant version of the minimum-energy estimator. Specifically, to consider adversarial attacks or artifacts associated with the measurement process, since the former approach is consistent with the fact that (adversarial) attacks on sensors often do not follow any particular dynamic or stochastic characterization.

Last but not least, it would be crucial to understand how to design filterlike approaches that amalgamate the problems of simultaneous system identification and estimation suitable for the deployment in real-time CNS.

13.3. Closed-loop control

Very rarely in practical settings do we have deterministic fractional-order models. As we saw, neural signals are particularly prone to artifacts from outside the brain. Furthermore, stabilizing the underlying models in the presence of disturbances becomes relevant in the treatment of disorders like epilepsy, Parkinson's, or Alzheimer's disease.

In recent years, there have been increasing research efforts into finding possible therapies for the aforementioned using neurofeedback (Marzbani et al., 2016). Future work, therefore, should focus on developing controllers and observers for fractional-order systems with the associated process and measurement noise and investigating the possible existence of separation principle-like results akin to those already existing in the field of linear stochastic control theory.

Another direction of work entails deriving robustness guarantees for controlling discrete-time fractional-order systems using an inner-outer loop control strategy. Specifically, in this context, we seek to discover the advantages and disadvantages of truncating a discrete-time fractional-order systems according to a given truncation horizon, thus approximating the fractional-order systems as an augmented LTI system and performing model predictive control with the same.

Additionally, one could also rely on some tools from robust control, namely integral quadratic constraints (IQCs) (Megretski and Rantzer, 1997). IQCs are, essentially, inequalities used to describe possible input-output signals resulting from a system component that is challenging to model because it is either nonlinear, time-varying, noisy, or switch stochastically or adversarially with time. A particular issue of interest will be to explore the trade-offs in performance when the fractional-order systems (which represents the inner loop) are written as an augmented LTI system due to a fixed truncation horizon versus when it is modeled as a non-Markovian nonlinearity with IQCs characterizing the same.

Additionally, although finite-time LTI truncations of fractional-order systems with constant truncation horizons are considered in this paper,

fractional-order systems inherently possess infinite long-term memory. The question that is an immediate consequence of the latter fact is whether the theory of linear control systems in infinite dimensions (Curtain and Zwart, 2012) can be used to provide key insights into control-theoretic properties such as controllability, observability, and stabilizability for such systems. While there have been some preliminary works in this direction (Baleanu et al., 2019; Zitane et al., 2020; Wei et al., 2019d; Sabatier, 2021). Consequently, future work must consist of using mathematical techniques used in the analysis of partial and delay differential equations, in particular, operator equations and C_0 -semigroup theory (Bamieh et al., 2002) for fractional-order systems.

From an engineering or applied control point-of-view, it is important to pinpoint some limitations and drawbacks of current event-triggered open-loop stimulation strategies (i.e., they can be inefficient or even cause seizure-like activity). Consequently, it serves as a call for action from neurophysiologists and engineers that work with neurostimulation (as well as deep brain stimulation) devices, towards validation in *in vitro* and *in vivo* scenarios. That said, the advances in computational processing power made in the last 10-20 years have made the prospects of turning into reality technology that was theoretically devised and previously impossible to implement in real-life. MPC and fractional-order systems-based technologies both fall under this category and have thus been significantly overlooked in the industry. However, both are growing in popularity amongst several research communities, and some predict a considerably more widespread impact than originally thought.

Notwithstanding, the validation is insufficient to establish a framework since several foundational problems need to be addressed. Specifically, the robustness of the stimulation strategies concerning the parameters of the models (e.g., the dynamics and the stimuli deployed, as well as the approximations considered to attain real-time stimulation) in devices with low storage, and limited battery and computation capabilities. Towards this goal, only transdisciplinary work between scientists and engineers will lead to success that ultimately will be reflected in the quality of life improvement of patients with neurological disorders (e.g., epilepsy).

References

Adams, J.L., Hartley, T.T., Lorenzo, C.F., 2006. Fractional-order system identification using complex order-distributions, in: Proc. 2nd IFAC Work-

- shop Fractional Differentiation and its Appl., Porto, Portugal. pp. 200–205.
- Agrawal, O.P., 2002. Formulation of euler–lagrange equations for fractional variational problems. Journal of Mathematical Analysis and Applications 272, 368–379.
- Agrawal, O.P., 2004. A general formulation and solution scheme for fractional optimal control problems. Nonlinear Dynamics 38, 323–337.
- Agrawal, O.P., Baleanu, D., 2007. A hamiltonian formulation and a direct numerical scheme for fractional optimal control problems. Journal of Vibration and Control 13, 1269–1281.
- Agrawal, O.P., Defterli, O., Baleanu, D., 2010. Fractional optimal control problems with several state and control variables. Journal of Vibration and Control 16, 1967–1976.
- Aguiar, A.P., Hespanha, J.P., 2006. Minimum-energy state estimation for systems with perspective outputs. IEEE Transactions on Automatic Control 51, 226–241.
- Alessandretti, A., Aguiar, A.P., Hespanha, J.P., Valigi, P., 2011. A minimum energy solution to monocular simultaneous localization and mapping, in: Proc. 50th IEEE Conf. Decision and Control held jointly with the Eur. Control Conf., Orlando, FL, USA. pp. 4566–4571.
- Alessandretti, A., Pequito, S., Pappas, G.J., Aguiar, A.P., 2020. Finite-dimensional control of linear discrete-time fractional-order systems. Automatica 115.
- Almeida, R., Torres, D.F., 2015. A discrete method to solve fractional optimal control problems. Nonlinear Dynamics 80, 1811–1816.
- Ashourvan, A., et al., 2020. Model-based design for seizure control by stimulation. J. Neural Eng. 17.
- Balachandran, K., Govindaraj, V., Ortigueira, M.D., Rivero, M., Trujillo, J.J., 2013. Observability and controllability of fractional linear dynamical systems. IFAC Proceedings Volumes 46, 893–898.

- Balakrishnan, S., Wainwright, M.J., Yu, B., 2017. Statistical guarantees for the EM algorithm: From population to sample-based analysis. Ann. Statist. 45, 77–120.
- Baleanu, D., Defterli, O., Agrawal, O.P., 2009. A central difference numerical scheme for fractional optimal control problems. Journal of Vibration and Control 15, 583–597.
- Baleanu, D., Diethelm, K., Scalas, E., Trujillo, J.J., 2012. Fractional calculus: models and numerical methods. volume 3. World Scientific.
- Baleanu, D., Fedorov, V.E., Gordievskikh, D.M., Taş, K., 2019. Approximate controllability of infinite-dimensional degenerate fractional order systems in the sectorial case. Mathematics 7.
- Baleanu, D., Güvenç, Z.B., Machado, J.T., et al., 2010. New trends in nanotechnology and fractional calculus applications. Springer.
- Baleanu, D., Machado, J.A.T., Luo, A.C., 2011. Fractional Dynamics and Control. Springer, New York, NY, USA.
- Bamieh, B., Paganini, F., Dahleh, M.A., 2002. Distributed control of spatially invariant systems. IEEE Transactions on Automatic Control 47, 1091–1107.
- Bargmann, C., Newsome, W., Anderson, A., Brown, E., Deisseroth, K., Donoghue, J., MacLeish, P., Marder, E., Normann, R., Sanes, J., et al., 2014. Brain 2025: a scientific vision. Brain Research through Advancing Innovative Neurotechnologies (BRAIN) Working Group Report to the Advisory Committee to the Director, NIH.
- Bassett, D.S., Sporns, O., 2017. Network neuroscience. Nature neuroscience 20, 353–364.
- Benzaouia, A., Hmamed, A., Mesquine, F., Benhayoun, M., Tadeo, F., 2014. Stabilization of continuous-time fractional positive systems by using a lyapunov function. IEEE Transactions on Automatic Control 59, 2203–2208.
- Bequette, B.W., 2013. Algorithms for a closed-loop artificial pancreas: The case for model predictive control. J. Diabetes Sci. and Technol. 7, 1632–1643. doi:10.1177/193229681300700624.

- Birs, I., Muresan, C., Nascu, I., Ionescu, C., 2019. A survey of recent advances in fractional order control for time delay systems. IEEE Access 7, 30951–30965.
- Biswas, R.K., Sen, S., 2011. Fractional optimal control problems with specified final time. Journal of computational and nonlinear dynamics 6.
- Bogdan, P., 2015. Mathematical modeling and control of multifractal workloads for data-center-on-a-chip optimization, in: Proceedings of the 9th International Symposium on Networks-on-Chip, pp. 1–8.
- Bogdan, P., Jain, S., Goyal, K., Marculescu, R., 2012a. Implantable pace-makers control and optimization via fractional calculus approaches: A cyber-physical systems perspective, in: 2012 IEEE/ACM Third International Conference on Cyber-Physical Systems, IEEE. pp. 23–32.
- Bogdan, P., Jain, S., Marculescu, R., 2013a. Pacemaker control of heart rate variability: A cyber physical system perspective. ACM Transactions on Embedded Computing Systems (TECS) 12, 1–22.
- Bogdan, P., Marculescu, R., 2011. Towards a science of cyber-physical systems design, in: 2011 IEEE/ACM second international conference on cyber-physical systems, IEEE. pp. 99–108.
- Bogdan, P., Marculescu, R., Jain, S., 2013b. Dynamic power management for multidomain system-on-chip platforms: An optimal control approach. ACM Transactions on Design Automation of Electronic Systems (TO-DAES) 18, 1–20.
- Bogdan, P., Marculescu, R., Jain, S., Gavila, R.T., 2012b. An optimal control approach to power management for multi-voltage and frequency islands multiprocessor platforms under highly variable workloads, in: 2012 IEEE/ACM Sixth International Symposium on Networks-on-Chip, IEEE. pp. 35–42.
- Bonilla, B., Rivero, M., Rodríguez-Germá, L., Trujillo, J.J., 2007. Fractional differential equations as alternative models to nonlinear differential equations. Applied Mathematics and computation 187, 79–88.

- Bonnabel, S., Slotine, J.J., 2015. A contraction theory-based analysis of the stability of the deterministic extended Kalman filter. IEEE Transactions on Automatic Control 60, 565–569.
- Buchstaller, D., Liu, J., French, M., 2020. The deterministic interpretation of the Kalman filter. Int. J. Control doi:10.1080/00207179.2020.1755895.
- Busłowicz, M., Ruszewski, A., 2013. Necessary and sufficient conditions for stability of fractional discrete-time linear state-space systems. Bulletin of the Polish Academy of Sciences. Technical Sciences 61.4.
- Cao, Q., Ramos, G., Bogdan, P., Pequito, S., 2019. The actuation spectrum of spatiotemporal networks with power-law time dependencies. Advances in Complex Systems 22, 1950023.
- Cao, Y., Li, Y., Ren, W., Chen, Y., 2009. Distributed coordination of networked fractional-order systems. IEEE Transactions on Systems, Man, and Cybernetics, Part B (Cybernetics) 40, 362–370.
- Caponetto, R., 2010. Fractional order systems: modeling and control applications. volume 72. World Scientific.
- Carmena, J., Sajda, P., Robinson, J., 2019. Future neural therapeutics: Closed-loop control of neural activity technology roadmap white paper.
- Chatterjee, S., Alessandretti, A., Aguiar, A.P., Pequito, S., 2021. Discrete-time fractional-order dynamical networks minimum-energy state estimation. arXiv preprint arXiv:2104.09409.
- Chatterjee, S., Pequito, S., 2019. Dealing with State Estimation in Fractional-Order Systems under Artifacts, in: Proceedings of the 2019 American Control Conference, IEEE. pp. 878–883.
- Chatterjee, S., Pequito, S., 2021. On learning discrete-time fractional-order dynamical systems. arXiv preprint arXiv:2103.14975.
- Chatterjee, S., Romero, O., Ashourvan, A., Pequito, S., 2020. Fractional-order model predictive control as a framework for electrical neurostimulation in epilepsy. J. Neural Eng. 17.

- Chatterjee, S., Romero, O., Pequito, S., 2019. A separation principle for discrete-time fractional-order dynamical systems and its implications to closed-loop neurotechnology. IEEE Control Syst. Lett. 3, 691–696. doi:10.1109/LCSYS.2019.2917164.
- Chavarriaga, R., 2020. Standards roadmap: Neurotechnologies for brain-machine interfacing.
- Chen, W., Sun, H., Zhang, X., Korošak, D., 2010. Anomalous diffusion modeling by fractal and fractional derivatives. Computers & Math. with Appl. 59, 1754–1758.
- Chen, Y., 2010. Fractional calculus, delay dynamics and networked control systems, in: Proceedings of the 2010 3rd International Symposium on Resilient Control Systems, IEEE. pp. 58–63.
- Chen, Y., Ahn, H.S., Podlubny, I., 2005. Robust stability check of fractional order linear time invariant systems with interval uncertainties, in: IEEE International Conference Mechatronics and Automation, 2005, IEEE. pp. 210–215.
- Chen, Y., Moore, K.L., Vinagre, B.M., Podlubny, I., 2004. Robust pid controller autotuning with a phase shaper, in: First IFAC workshop on fractional differentiation and its applications, Citeseer. pp. 162–167.
- Chen, Y., Petras, I., Xue, D., 2009. Fractional order control-a tutorial, in: 2009 American control conference, IEEE. pp. 1397–1411.
- Curtain, R.F., Zwart, H., 2012. An Introduction to Infinite-Dimensional Linear Systems Theory. volume 21. Springer-Verlag, New York, NY, USA.
- Cybenko, G., 1989. Approximation by superpositions of a sigmoidal function. Math. Control, Signals and Syst. 2, 303–314.
- Dastjerdi, A.A., Vinagre, B.M., Chen, Y., HosseinNia, S.H., 2019. Linear fractional order controllers; a survey in the frequency domain. Annual Reviews in Control 47, 51–70.
- Dzielinski, A., Sierociuk, D., 2005. Adaptive feedback control of fractional order discrete state-space systems, in: Proc. Int. Conf. Comput. Intell. for Model., Control and Automat. and Int. Conf. Intell. Agents, Web Technol. and Internet Commerce, Vienna, Austria. pp. 804–809.

- Dzieliński, A., Sierociuk, D., 2008. Stability of discrete fractional order statespace systems. Journal of Vibration and Control 14, 1543–1556.
- Dzieliński, A., Sierociuk, D., Sarwas, G., Petráš, I., Podlubny, I., Škovránek, T., 2011. Identification of the fractional-order systems: A frequency domain approach. Acta Montanistica Slovaca 16, 26–33.
- Efe, M.Ö., 2011. Fractional order systems in industrial automation—a survey. IEEE Transactions on Industrial Informatics 7, 582–591.
- Fagnani, F., Willems, J.C., 1997. Deterministic Kalman filtering in a behavioral framework. Syst. & Control Lett. 32, 301–312.
- Fairclough, S.H., Lotte, F., 2020. Grand challenges in neurotechnology and system neuroergonomics. Frontiers in Neuroergonomics 1, 2.
- Flandrin, P., 1992. Wavelet analysis and synthesis of fractional Brownian motion. IEEE Transactions on Information Theory 38, 910–917.
- Fleming, W.H., 1997. Deterministic nonlinear filtering. Annali della Scuola Normale Superiore di Pisa, Classe di Scienze Ser. 4, 25, 435–454.
- Foucart, S., Rauhut, H., 2013. A Mathematical Introduction to Compressive Sensing. Applied and Numerical Harmonic Analysis, Birkhäuser, New York, NY, USA.
- Frederico, G.S., Torres, D.F., 2007. A formulation of noether's theorem for fractional problems of the calculus of variations. Journal of Mathematical Analysis and Applications 334, 834–846.
- Frederico, G.S., Torres, D.F., 2008. Fractional conservation laws in optimal control theory. Nonlinear Dynamics 53, 215–222.
- Funahashi, K.I., 1989. On the approximate realization of continuous mappings by neural networks. Neural Netw. 2, 183–192.
- Ghorbani, M., Bogdan, P., 2013. A cyber-physical system approach to artificial pancreas design, in: Proc. 9th IEEE/ACM/IFIP Int. Conf. Hardware/Software Codesign and Syst. Synthesis, Montreal, QC, Canada. pp. 1–10.

- Ghorbani, M., Bogdan, P., 2014. Reducing risk of closed loop control of blood glucose in artificial pancreas using fractional calculus, in: 2014 36th Annual International Conference of the IEEE Engineering in Medicine and Biology Society, IEEE. pp. 4839–4842.
- Ghorbani, M., Wang, Y., Xue, Y., Pedram, M., Bogdan, P., 2014. Prediction and control of bursty cloud workloads: a fractal framework, in: Proceedings of the 2014 international conference on hardware/software codesign and system synthesis, pp. 1–9.
- Gibson, S., Ninness, B., 2005. Robust maximum-likelihood estimation of multivariable dynamic systems. Automatica 41, 1667–1682.
- Goldberger, A.L., et al., 2000. PhysioBank, PhysioToolkit, and PhysioNet: Components of a new research resource for complex physiologic signals. Circulation 101, e215–e220.
- Goodrich, C., Peterson, A.C., 2015. Discrete fractional calculus. volume 1350. Springer.
- Grant, M., Boyd, S., 2008. Graph implementations for nonsmooth convex programs, in: Blondel, V., Boyd, S., Kimura, H. (Eds.), Recent Advances in Learning and Control. Springer, London, United Kingdom. Lecture Notes in Control and Information Sciences, pp. 95–110.
- Grant, M., Boyd, S., 2014. CVX: Matlab software for disciplined convex programming, version 2.1. http://cvxr.com/cvx. Accessed: Jul. 18, 2021.
- Guermah, S., Djennoune, S., Bettayeb, M., 2008. Controllability and observability of linear discrete-time fractional-order systems. International Journal of Applied Mathematics & Computer Science 18.
- Gupta, G., Pequito, S., Bogdan, P., 2018a. Dealing with unknown unknowns: Identification and selection of minimal sensing for fractional dynamics with unknown inputs, in: Proc. 2018 Amer. Control Conf., Milwaukee, WI, USA. pp. 2814–2820.
- Gupta, G., Pequito, S., Bogdan, P., 2018b. Re-thinking EEG-based non-invasive brain interfaces: Modeling and analysis, in: Proc. ACM/IEEE 9th Int. Conf. Cyber-Physical Syst., Porto, Portugal. pp. 275–286.

- Gupta, G., Pequito, S., Bogdan, P., 2019. Learning latent fractional dynamics with unknown unknowns, in: 2019 American Control Conference (ACC), IEEE. pp. 217–222.
- Gupta, G., Yin, C., Deshmukh, J.V., Bogdan, P., 2021. Non-markovian reinforcement learning using fractional dynamics. arXiv preprint arXiv:2107.13790.
- Ha, T.N., Aguiar, A.P., 2018. Cooperative joint estimation and localization using mobile multi-agent systems: A minimum energy estimator approach, in: Proc. 16th Eur. Control Conf., Limassol, Cyprus. pp. 2224–2229.
- Haring, M., Johansen, T.A., 2020. On the stability bounds of Kalman filters for linear deterministic discrete-time systems. IEEE Transactions on Automatic Control 65, 4434–4439. doi:10.1109/TAC.2020.2966150.
- Hassani, V., Aguiar, A.P., Athans, M., Pascoal, A.M., 2009. Multiple model adaptive estimation and model identification using a minimum energy criterion, in: Proc. 2009 Amer. Control Conf., St. Louis, MO, USA. pp. 518–523.
- Hijab, O., 1980. Minimum energy estimation. Ph.D. thesis. Univ. California. Berkeley.
- Hornik, K., Stinchcombe, M., White, H., 1989. Multilayer feedforward networks are universal approximators. Neural Netw. 2, 359–366.
- Hutter, C., Gül, R., Bölcskei, H., 2021. Metric entropy limits on recurrent neural network learning of linear dynamical systems. arXiv:2105.02556.
- Jansen, B.H., Rit, V.G., 1995. Electroencephalogram and visual evoked potential generation in a mathematical model of coupled cortical columns. Biol. Cybern. 73, 357–366.
- Jansen, B.H., Zouridakis, G., Brandt, M.E., 1993. A neurophysiologically-based mathematical model of flash visual evoked potentials. Biol. Cybern. 68, 275–283.
- Jirsa, V.K., Stacey, W.C., Quilichini, P.P., Ivanov, A.I., Bernard, C., 2014. On the nature of seizure dynamics. Brain 137, 2210–2230.

- Khambhati, A.N., Davis, K.A., Oommen, B.S., Chen, S.H., Lucas, T.H., Litt, B., Bassett, D.S., 2015. Dynamic network drivers of seizure generation, propagation and termination in human neocortical epilepsy. PLoS Computational Biology 11.
- Kilbas, A., Trujillo, J., 2001. Differential equations of fractional order: methods results and problem—i. Applicable analysis 78, 153–192.
- Kilbas, A., Trujillo, J., 2002. Differential equations of fractional order: methods, results and problems. ii. Applicable Analysis 81, 435–493.
- Kilbas, A.A., Srivastava, H.M., Trujillo, J.J., 2006. Theory and applications of fractional differential equations. volume 204. elsevier.
- Kokotovic, P.V., 1992. The joy of feedback: nonlinear and adaptive. IEEE Control Systems Magazine 12, 7–17.
- Krener, A.J., 2003. The convergence of the minimum energy estimator, in: Kang, W., Xiao, M., Borges, C. (Eds.), New Trends in Nonlinear Dyn. and Control and their Appl.. Springer-Verlag, Berlin, Heidelberg, Germany. volume 295, pp. 187–208.
- Kyriakis, P., Pequito, S., Bogdan, P., 2020. On the effects of memory and topology on the controllability of complex dynamical networks. Scientific Reports 10, 1–13.
- LeDoux, J., 1998. The emotional brain: The mysterious underpinnings of emotional life. Simon and Schuster.
- Lewis, T., 2020. Elon musk's pig-brain implant is still a long way from 'solving paralysis'. Scientific American, online.
- Li, A., Inati, S., Zaghloul, K., Sarma, S., 2017. Fragility in epileptic networks: the epileptogenic zone, in: 2017 American Control Conference (ACC), IEEE. pp. 2817–2822.
- Li, Y., Chen, Y., Podlubny, I., 2009. Mittag-leffler stability of fractional order nonlinear dynamic systems. Automatica 45, 1965–1969.
- Li, Y., Chen, Y., Podlubny, I., 2010. Stability of fractional-order nonlinear dynamic systems: Lyapunov direct method and generalized mittag—leffler stability. Computers & Mathematics with Applications 59, 1810–1821.

- Ljung, L., 1999. System Identification: Theory for the User. Prentice-Hall, Upper Saddle River, NJ, USA.
- Lozano, R., Brogliato, B., et al., 1992. Adaptive control of robot manipulators with flexible joints. IEEE Transactions on Automatic Control 37, 174–181.
- Lundstrom, B.N., Higgs, M.H., Spain, W.J., Fairhall, A.L., 2008. Fractional differentiation by neocortical pyramidal neurons. Nature Neuroscience 11, 1335–1342.
- Magin, R.L., 2006. Fractional Calculus in Bioengineering. Begell House, Redding, CT, USA.
- Mahmoud, M., 2012. Advances in Discrete Time Systems. BoD–Books on Demand.
- Markram, H., 2012. The human brain project. Scientific American 306, 50–55.
- Martinet, L.E., et al., 2017. Human seizures couple across spatial scales through travelling wave dynamics. Nature Commun. 8.
- Marzbani, H., Marateb, H.R., Mansourian, M., 2016. Neurofeedback: A comprehensive review on system design, methodology and clinical applications. Basic and Clin. Neuroscience 7, 143–158.
- Matignon, D., 1996. Stability results for fractional differential equations with applications to control processing, in: Computational engineering in systems applications, Citeseer. pp. 963–968.
- Matignon, D., d'Andréa Novel, B., 1996. Some results on controllability and observability of finite-dimensional fractional differential systems, in: Computational engineering in systems applications, Citeseer. pp. 952–956.
- Matušu, R., 2011. Application of fractional order calculus to control theory. International journal of mathematical models and methods in applied sciences 5, 1162–1169.
- Megretski, A., Rantzer, A., 1997. System analysis via integral quadratic constraints. IEEE Transactions on Automatic Control 42, 819–830.

- Miljković, N., Popović, N., Djordjević, O., Konstantinović, L., Šekara, T.B., 2017. ECG artifact cancellation in surface EMG signals by fractional order calculus application. Comput. Methods and Programs in Biomedicine 140, 259–264.
- Monje, C.A., Chen, Y., Vinagre, B.M., Xue, D., Feliu-Batlle, V., 2010. Fractional-order systems and controls: fundamentals and applications. Springer Science & Business Media.
- Monje, C.A., Vinagre, B.M., Feliu, V., Chen, Y., 2008. Tuning and autotuning of fractional order controllers for industry applications. Control engineering practice 16, 798–812.
- Moon, F.C., 2008. Chaotic and Fractal Dynamics: An Introduction for Applied Scientists and Engineers. Wiley, Hoboken, NJ, USA.
- Moratti, S., Patterson, D., 2014. Adverse psychological effects to deep brain stimulation: Overturning the question. Amer. J. Bioethics Neuroscience 5, 62–64.
- Mortensen, R.E., 1968. Maximum-likelihood recursive nonlinear filtering. J. Optim. Theory Appl. 2, 386–394.
- Mozyrska, D., Pawłuszewicz, E., 2012. Fractional discrete-time linear control systems with initialisation. International Journal of Control 85, 213–219.
- Najar, S., Abdelkrim, M.N., Abdelhamid, M., Mohamed, A., 2009. Discrete fractional Kalman filter, in: Proc. 2nd IFAC Conf. Intell. Control Syst. Signal Process., Istanbul, Turkey. pp. 520–525.
- Nemati, S., Lima, P.M., Torres, D.F., 2019. A numerical approach for solving fractional optimal control problems using modified hat functions. Communications in Nonlinear Science and Numerical Simulation 78, 104849.
- Oldham, K., Spanier, J., 1974. The fractional calculus theory and applications of differentiation and integration to arbitrary order. Elsevier.
- Ortigueira, M.D., 2000. Introduction to fractional linear systems. part 1: Continuous-time case. IEE Proceedings-Vision, Image and Signal Processing 147, 62–70.

- Pequito, S., Aguiar, A.P., Gomes, D.A., 2009. The entropy penalized minimum energy estimator, in: Proc. 48th IEEE Conf. Decis. and Control held jointly with the 28th Chin. Control Conf., Shanghai, China. pp. 1285–1290.
- Pequito, S., Ashourvan, A., Bassett, D., Litt, B., Pappas, G.J., 2017. Spectral control of cortical activity, in: 2017 American Control Conference (ACC), IEEE. pp. 2785–2791.
- Pequito, S., Bogdan, P., Pappas, G.J., 2015. Minimum number of probes for brain dynamics observability, in: Proc. 54th IEEE Conf. Decis. and Control, Osaka, Japan. pp. 306–311. doi:10.1109/CDC.2015.7402218.
- Petráš, I., 2011. Fractional-order chaotic systems, in: Fractional-Order Nonlinear Systems: Modeling, Analysis and Simulation. Springer-Verlag, Berlin, Heidelberg, Germany, pp. 103–184.
- Petráš, I., 2021. Novel fractional-order model predictive control: State-space approach. IEEE Access 9, 92769–92775.
- Podlubny, I., 1998. Fractional differential equations: an introduction to fractional derivatives, fractional differential equations, to methods of their solution and some of their applications. Elsevier.
- Podlubny, I., 1999. Fractional-order systems and pi/sup/spl lambda//d/sup/spl mu//-controllers. IEEE Transactions on automatic control 44, 208–214.
- Presigny, C., Fallani, F.D.V., 2021. Multiscale modeling of brain network organization. arXiv preprint arXiv:2111.13473.
- Qin, S.J., Badgwell, T.A., 2003. A survey of industrial model predictive control technology. Control Eng. Pract. 11, 733–764.
- Reed, E.A., Bogdan, P., Pequito, S., 2021. Quantification of fractional dynamical stability of eeg signals as a bio-marker for cognitive motor control. Frontiers in Control Engineering .
- Regalado, A., 2020. Elon musk's neuralink is neuroscience theater.
- Ren, W., Cao, Y., 2011. Distributed Coordination of Multi-agent Networks: Emergent Problems, Models, and Issues. volume 1. Springer.

- Riewe, F., 1996. Nonconservative lagrangian and hamiltonian mechanics. Physical Review E 53, 1890.
- Rivero, M., Rogosin, S.V., Tenreiro Machado, J.A., Trujillo, J.J., 2013. Stability of fractional order systems. Mathematical Problems in Engineering 2013.
- Rodgers, A., 2020. Neuralink is impressive tech, wrapped in musk hype.
- Sabatier, J., 2021. Fractional order models are doubly infinite dimensional models and thus of infinite memory: Consequences on initialization and some solutions. Symmetry 13.
- Sabatier, J., Agrawal, O.P., Machado, J.T., 2007. Advances in fractional calculus. volume 4. Springer.
- Sabatier, J., Farges, C., Merveillaut, M., Feneteau, L., 2012. On observability and pseudo state estimation of fractional order systems. Eur. J. Control 18, 260–271.
- Safarinejadian, B., Asad, M., Sadeghi, M.S., 2016. Simultaneous state estimation and parameter identification in linear fractional order systems using coloured measurement noise. Int. J. Control 89, 2277–2296. doi:10.1080/00207179.2016.1155237.
- Safarinejadian, B., Kianpour, N., Asad, M., 2018. State estimation in fractional-order systems with coloured measurement noise. Trans. Inst. Meas. Control 40, 1819–1835. doi:10.1177/0142331217691219.
- Scalas, E., Gorenflo, R., Mainardi, F., 2000. Fractional calculus and continuous-time finance. Physica A: Statistical Mechanics and its Applications 284, 376–384.
- Schalk, G., McFarland, D.J., Hinterberger, T., Birbaumer, N., Wolpaw, J.R., 2004. BCI2000: A general-purpose brain-computer interface (BCI) system. IEEE Transactions on Biomedical Engineering 51, 1034–1043. doi:10.1109/TBME.2004.827072.
- Schön, T.B., Wills, A., Ninness, B., 2011. System identification of nonlinear state-space models. Automatica 47, 39–49.

- Shahin, A., Ahmed, E., Omar, Y.A., 2009. On fractional order quantum mechanics. International Journal of Nonlinear Science 8, 469–472.
- Shalalfeh, L., Bogdan, P., Jonckheere, E.A., 2020. Fractional dynamics of pmu data. IEEE Transactions on Smart Grid 12, 2578–2588.
- Shlesinger, M.F., Zaslavsky, G.M., Klafter, J., 1993. Strange kinetics. Nature 363, 31–37.
- Sierociuk, D., Dzieliński, A., 2006. Fractional Kalman filter algorithm for the states, parameters and order of fractional system estimation. Int. J. Appl. Math. Comput. Sci. 16, 129–140.
- Söderström, T., Stoica, P., 1989. System Identification. Prentice-Hall, Englewood Cliffs, NJ, USA.
- Soltan, A., Xia, L., Jackson, A., Chester, G., Degenaar, P., 2018. Fractional order PID system for suppressing epileptic activities, in: Proc. 2018 IEEE Int. Conf. Appl. Syst. Invention, Chiba, Japan. pp. 338–341.
- Sopasakis, P., Sarimveis, H., 2017. Stabilising model predictive control for discrete-time fractional-order systems. Automatica 75, 24–31.
- Steyn-Ross, M.L., Steyn-Ross, D.A., Sleigh, J.W., 2013. Interacting Turing-Hopf instabilities drive symmetry-breaking transitions in a mean-field model of the cortex: A mechanism for the slow oscillation. Phys. Rev. X 3.
- Swerling, P., 1971. Modern state estimation methods from the viewpoint of the method of least squares. IEEE Transactions on Automatic Control 16, 707–719.
- Teich, M.C., Heneghan, C., Lowen, S.B., Ozaki, T., Kaplan, E., 1997. Fractal character of the neural spike train in the visual system of the cat. J. Opt. Soc. Amer. 14, 529–546.
- Thurner, S., Windischberger, C., Moser, E., Walla, P., Barth, M., 2003. Scaling laws and persistence in human brain activity. Physica A: Stat. Mech. Appl. 326, 511–521.
- Tjärnström, F., 1999. The Use of Bootstrap in System Identification. Linköping University Electronic Press, Linköping, Sweden.

- Torres, D.F., Malinowska, A.B., 2012. Introduction to the fractional calculus of variations. World Scientific Publishing Company.
- Turcott, R.G., Teich, M.C., 1996. Fractal character of the electrocardiogram: Distinguishing heart-failure and normal patients. Ann. Biomed. Eng. 24, 269–293.
- Tzoumas, V., Xue, Y., Pequito, S., Bogdan, P., Pappas, G.J., 2018. Selecting sensors in biological fractional-order systems. IEEE Transactions on Control of Network Systems 5, 709–721.
- Valério, D., Trujillo, J.J., Rivero, M., Machado, J.T., Baleanu, D., 2013. Fractional calculus: A survey of useful formulas. The European Physical Journal Special Topics 222, 1827–1846.
- Van Essen, D.C., Smith, S.M., Barch, D.M., Behrens, T.E., Yacoub, E., Ugurbil, K., Consortium, W.M.H., et al., 2013. The wu-minn human connectome project: an overview. Neuroimage 80, 62–79.
- Vinagre, B., Podlubny, I., Hernandez, A., Feliu, V., 2000. Some approximations of fractional order operators used in control theory and applications. Fractional calculus and applied analysis 3, 231–248.
- Vinagre, B.M., Calderón, A.J., 2006. On fractional sliding mode control, in: Proc. 7th Portuguese Conf. Autom. Control (CONTROLO'06).
- Wang, J., Niebur, E., Hu, J., Li, X., 2016. Suppressing epileptic activity in a neural mass model using a closed-loop proportional-integral controller. Scientific Rep. 6.
- Wei, W., Wei, X., Xia, P., Zuo, M., Shen, D., 2019a. Seizure control by a learning type active disturbance rejection approach. IEEE Access 7, 164792–164802.
- Wei, W., Wei, X., Zuo, M., 2019b. Control of epileptiform waves in a neural mass model, in: Proc. 2019 Chin. Control Conf., Guangzhou, China. pp. 6860–6864.
- Wei, W., Wei, X., Zuo, M., Yu, T., Li, Y., 2019c. Seizure control in a neural mass model by an active disturbance rejection approach. Int. J. Adv. Robot. Syst. 16, 1–15.

- Wei, Y., Chen, Y., Wang, J., Wang, Y., 2019d. Analysis and description of the infinite-dimensional nature for nabla discrete fractional order systems. Commun. Nonlinear Sci. Numer. Simul. 72, 472–492.
- Wendling, F., Bellanger, J.J., Bartolomei, F., Chauvel, P., 2000. Relevance of nonlinear lumped-parameter models in the analysis of depth-EEG epileptic signals. Biol. Cybern. 83, 367–378.
- Wendling, F., Benquet, P., Bartolomei, F., Jirsa, V., 2016. Computational models of epileptiform activity. J. Neuroscience Methods 260, 233–251.
- Werner, G., 2010. Fractals in the nervous system: Conceptual implications for theoretical neuroscience. Front. Physiol. 1.
- West, B.J., 2014. Colloquium: Fractional calculus view of complexity: A tutorial. Reviews of Modern Physics 86, 1169.
- West, B.J., 2016. Fractional Calculus View of Complexity: Tomorrow's Science. CRC Press, Boca Raton, FL, USA.
- West, B.J., Turalska, M., Grigolini, P., 2015. Fractional calculus ties the microscopic and macroscopic scales of complex network dynamics. New Journal of Physics 17, 045009.
- West, B.J., Turalska, M., Grigolini, P., 2016. Networks of Echoes. Springer International Publishing AG, Cham, Switzerland.
- Willems, J.C., 2004. Deterministic least squares filtering. J. Econometrics 118, 341–373.
- Wu, C., Yang, C., Zhao, H., Zhu, J., 2016. On the convergence of the EM algorithm: A data-adaptive analysis. arXiv:1611.00519.
- Xia, L., Soltan, A., Zhang, X., Jackson, A., Tessier, R., Degenaar, P., 2019. Closed-loop proportion-derivative control of suppressing seizures in a neural mass model, in: Proc. 2019 IEEE Int. Symp. Circuits and Syst., Sapporo, Japan. pp. 1–5.
- Xue, Y., Bogdan, P., 2017. Constructing compact causal mathematical models for complex dynamics, in: Proc. 8th Int. Conf. Cyber-Physical Syst., Pittsburgh, PA, USA. pp. 97–107.

- Xue, Y., Pequito, S., Coelho, J.R., Bogdan, P., Pappas, G.J., 2016a. Minimum number of sensors to ensure observability of physiological systems: A case study, in: Proc. 54th Annu. Allerton Conf. Commun., Control, and Comput., Monticello, IL, USA. pp. 1181–1188.
- Xue, Y., Rodriguez, S., Bogdan, P., 2016b. A spatio-temporal fractal model for a CPS approach to brain-machine-body interfaces, in: Proc. 2016 Des., Automat. & Test in Europe Conf. & Exhib., Dresden, Germany. pp. 642–647.
- Yan, B., Yin, M., Sarkar, P., 2017. Convergence of gradient EM on multicomponent mixture of Gaussians, in: Advances in Neural Inf. Process. Syst., Long Beach, CA, USA. pp. 6956–6966.
- Zaky, M.A., Machado, J.T., 2017. On the formulation and numerical simulation of distributed-order fractional optimal control problems. Communications in Nonlinear Science and Numerical Simulation 52, 177–189.
- Zames, G., Owen, J., 1993. A note on metric dimension and feedback in discrete time. IEEE Transactions on Automatic Control 38, 664–667.
- Zhang, X., Chen, Y., 2012. Remarks on fractional order control systems, in: 2012 American Control Conference (ACC), IEEE. pp. 5169–5173.
- Zitane, H., Boutoulout, A., Torres, D.F., 2020. The stability and stabilization of infinite dimensional Caputo-time fractional differential linear systems. Mathematics 8.